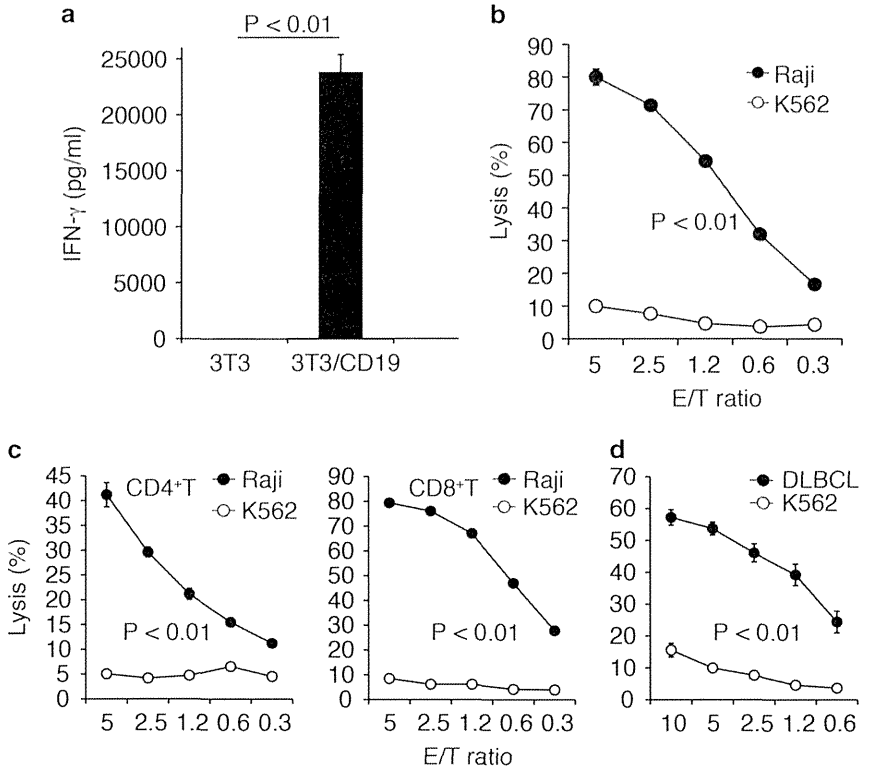

Figure 3. Antigen-specific effector functions of CD19-CAR T-cells *in vitro*. (**a**) IFN-γ secretion by CD19-CAR T-cells after co-culture with 3T3/CD19 or parental 3T3 cells. (**b**) Cytotoxicity of CD19-CAR T-cells against Raji and K562 cells in Calcein-AM release assays. K562 cells served as $CD19^-$ targets. (**c**) Cytotoxic activities in CD4- and CD8-sorted T-cells. (**d**) Cytotoxicity against primary $CD19^+$ diffuse large B-cell lymphoma (DLBCL) cells. Values show the mean ± s.d. of triplicate wells.

$CD3^+$ SB-engineered T-cells (19–65%; day 1).[13,20] After 3 weeks of expansion, stable and robust CD19-CAR expression was detected in engineered T-cells (~95%; Figure 2a, lower), comparable to that observed in SB- or PB-engineered T-cells with CD19-CAR (51–98%) after 3 weeks of expansion with antigen stimulation.[10,13,20] Improvements in vector design and delivery should yield even better results. Peng *et al.*[21] showed that a green fluorescent protein (GFP)-encoded SB transposon exhibited >50% transduction without antigen stimulation in primary T-cells in the presence of an mRNA-encoded transposase. Additionally, SB100X, which encodes a hyperactive SB transposase, exhibited improved transposition activity and enhanced T-cell gene transfer efficiency.[22] Thus future development of the hyperactive *Tol2* transposase and its RNA delivery may improve the generation of CD19-CAR T-cells.

Some retroviral vectors integrate near transcription start sites and so have the potential to cause insertional mutagenesis.[23] However, as yet there have been no reports that retroviral vectors have caused adverse events in T-cells.[24] *Tol2* transposons preferentially integrate around transcription start sites, CpG islands and DNaseI hypersensitive sites.[25] We mapped the integration sites of *Tol2*- and retrovirus vector-engineered T-cells with CD19-CAR and showed that their target sequences did not overlap (Table 1). However, our sample size is too small to compare the exact integration profile of each vector, so further large-scale comparative analysis of integration sites will provide the necessary important information about the integration preference and safety of the vectors. Regardless of the vector system used, the development of safer transgene delivery systems has become an important area of study. To this end, AAV-based site-directed integration systems may be useful, because Rep proteins from AAV facilitate the integration of the viral genome into a specific locus (termed AAVS1) in chromosome 19.[26] This locus is one of the safe locations in the human genome for efficient and safe transgene expression.[27] Ammar *et al.*[28] demonstrated that fusion constructs consisting of Rep and *Tol2* transposase integrated marker genes from *Tol2* transposon donor plasmids near the AAVS1 locus, which may offer a safer transposon-based gene delivery system for human gene and cell therapy.

In the present study, we have demonstrated that the adoptive transfer of *Tol2*-engineered T-cells with CD19-CAR suppressed tumor growth in tumor-bearing mice and have shown enhanced tumor suppression of *Tol2*-engineered T-cells in combination with systemic IL-7 delivery. IL-7 has previously been used to enhance the anti-tumor effect of tumor specific-T-cells in preclinical and clinical studies and has acceptable toxicity profiles.[18] Furthermore, IL-7 preferentially maintains memory $CD4^+$ and $CD8^+$ T-cells over $CD4^+CD25^+Foxp3^+$ regulatory T-cells in clinical trials.[18] Therefore, IL-7 appears to be a potential adjuvant for engineered T-cell therapy.

The *Tol2* transposon system is a promising technology for gene transfer in mammalian cells, and its efficacy is comparable with other transposon systems, such as SB and PB transposons. *Tol2* also offers some advantages over SB, including a high cargo capacity and limited OPI, which are important characteristics for transposon-based gene therapy. With respect to cargo capacity and OPI, PB is similar to *Tol2*. Therefore, the simultaneous comparison of *Tol2* and PB, with or without various augmenting reagents (for example, PD-1 antibody or IL-7) in a characterized mouse model as described in this work, would help identify an optimal transposon system for immunogene therapy.

In conclusion, we used the *Tol2* transposon system to stably transfer CD19-CAR into primary human T-cells. We found that expanded T-cells contained one or two copies of *CD19-CAR* leading to efficient transgene expression and further

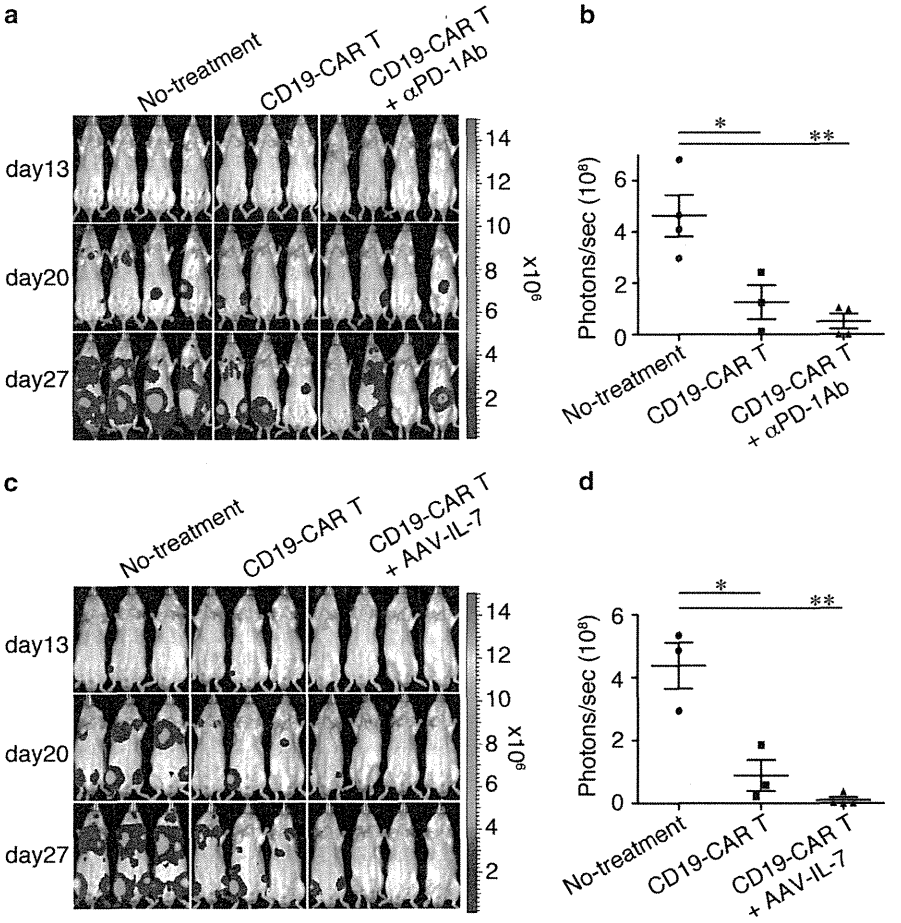

Figure 4. (**a**) Bioluminescent imaging of systemic Raji tumor progression in $Rag2^{-/-}\gamma c^{-/-}$ mice following T-cell infusion. Mice inoculated intravenously with Raji/Luc cells on day 0 were infused with CD19-CAR T-cells alone on day 3 (T-cell treatment group, $n=3$) or in combination with three intraperitoneal injections of an anti-PD-1 antibody ($n=4$), whereas mice in the control group did not receive T-cells ($n=4$). (**b**) Quantitative bioluminescence imaging on day 27 as shown in panel (**a**). (**c**) Raji tumor-bearing mice were infused with CD19-CAR T-cells alone ($n=3$) on day 3 or in combination with a single intramuscular injection of AAV-IL-7 ($n=4$). (**d**) Quantitative bioluminescence image on day 27 as shown in panel (**c**). Bioluminescent imaging was performed on days 13, 20 and 27. $^{*}P<0.05$, $^{**}P<0.01$.

demonstrated that they exhibited CD19-dependent anti-tumor effects *in vitro* and in a xenograft mouse model of human B-cell lymphoma. Our results indicate that the *Tol2* transposon system is a useful gene transfer platform and could be applied to CD19-CAR-based T-cell therapy for refractory B-cell malignancies.

MATERIALS AND METHODS

Plasmids

The *Tol2* transposon plasmid pT2AL200R175-CAGGS-EGFP has been described previously.[7] The *Tol2* transposon plasmid encoding CD19-specific CAR with CD28 and CD3ζ signaling domains (CD19-CAR) from the SFG-1928z retroviral vector[29] pTol2-CD19-CAR was generated by replacing the EGFP sequence of pT2AL200R175-CAGGS-EGFP with the CD19-CAR sequence. The *Tol2*-transposase plasmid pCAGGS-mT2TP carrying a modified transposase cDNA[5] with codons optimized for mammalian use was also transfected. The human IL-7 expression vector AAV-IL-7 was generated by ligating IL-7 cDNA into the pAAV-MCS vector (Agilent Technologies Inc., Palo Alto, CA, USA).

Recombinant AAV-IL-7 production

The recombinant AAV-IL-7 vector (serotype 1) was prepared as previously described,[30] and vector titers were measured using real-time PCR.[30]

PBLs and cell lines

PBLs from three healthy donors and a clinical sample from a patient with non-Hodgkin B-cell lymphoma were collected under a protocol approved by the Jichi Medical University Institutional Review Board, with written informed consent obtained from each donor. The mouse fibroblast NIH3T3 cell line expressing human CD19 (3T3/CD19)[31] was maintained in Dulbecco's modified Eagle's medium (Life Technologies, Carlsbad, CA, USA) supplemented with 10% fetal bovine serum (Sigma-Aldrich, St Louis, MO, USA). The human Burkitt lymphoma cell line Raji (Health Science Research Resources Bank, Osaka, Japan), Raji cells expressing luciferase (Raji/Luc)[15] and the human erythroleukemia cell line K562 (Riken BRC, Ibaraki, Japan) were also used. Cell lines were cultured in RPMI 1640 medium (Life Technologies) supplemented with 10% fetal bovine serum.

Transfection and expansion of T-cells

PBLs (5×10^6) were nucleofected with pTol2-CD19-CAR and pCAGGS-mT2TP (5 μg each) using the Human T-cell Nucleofector Kit and Amaxa Nucleofector II program U-014 (Lonza, Basel, Switzerland) on day 0. Transfected PBLs were transferred to X-Vivo 15 (Takara Bio, Shiga, Japan) supplemented with 5% human AB serum (NOVA Biologics, Oceanside, CA, USA) (T-cell complete medium) and cultured overnight. The next day, cells were stimulated with γ-irradiated (50 Gy) 3T3/CD19 cells at a 1:1 ratio

for selective propagation and cultured in T-cell complete medium supplemented with 1 nM recombinant human IL-2 (Life Technologies) in G-Rex10 culture flasks (Wilson Wolf Manufacturing Corporation, New Brighton, MN, USA). 3T3/CD19 cells were added to the T-cell cultures on days 1 and 8.

Flow cytometry

CD19-CAR surface expression on transduced T-cells was assessed using a biotin goat anti-mouse F(ab')-specific antibody, phycoerythrin–Streptavidin (Jackson Immunoresearch, West Grove, PA, USA) and fluorescein isothiocyanate anti-human CD3 (Biolegend, San Diego, CA, USA). Samples were analyzed using the BD LSR Fortessa with FACSDiva software (BD Biosciences, San Diego, CA, USA).

Western blotting

CD19-CAR protein expression was examined by western blotting using an anti-human CD3ζ antibody as described previously.[15]

Transgene copy number and integration sites

Transgene copy numbers were measured by real-time quantitative PCR using Thermal Cycler Dice Real Time System II (Takara Bio). Genomic DNA was isolated from CD19-CAR T-cells by a QIAamp DNA Mini Kit (Qiagen, Valencia, CA, USA) on days 21 and 29 after transduction. PCR was performed using a Cycleave PCR Core kit (Takara Bio) with sets of primers and probes specific for *CD19-CAR* and human *IFN-γ*. For *CD19-CAR*, these were the forward primer A: 5′-TGCACAGTGACTACATGAACA-3′; the reverse primer B: 5′-CGTC CTAGATTGAGCTCGTTA-3′; and probe: 5′-gctcc(A)gag-3′; for *IFN-γ*, these were the forward primer C: 5′-CAGGGTCACCTGACACATTCA-3′; the reverse primer D: 5′-ACTAGGCAGCCAACCTAAGC-3′; and probe: 5′-acaatgaac(A)ct-3′. Uppercase letters of probe sequences represent RNA bases. Serially diluted CD19-CAR and human IFN-γ plasmid standards (1 μl containing 6×10^{1}–3×10^{6} copies each) were used. Each standard curve (threshold cycle values versus copy numbers) is shown in Supplementary Figure S2 (day 29). The average *CD19-CAR* copy number per cell was calculated by normalizing to the endogenous number of diploid human *IFN-γ* copies.

Inverse PCR was performed as described previously[7] to identify the 3′ transposon junction sequence. Genomic DNA was digested with *Hpa* II and self-ligated. Integration junction sequences were amplified by two rounds of PCR. The primers for first-round PCR were: F1 (5′-TGGCGGCCTCGAGTGGCTGTTA-3′) and R1 (5′-CTCTA CAAATGTGGTATGGCTG-3′); those for second-round PCR were: F2 (5′-GTGAAGGGCGTCGTAGGTGTC-3′) and R2 (5′-GTATGGCTGATT ATGATCCTCTA-3′). Second-round PCR products were cloned into a pMD20-T vector (Takara Bio), which was then transformed into DH5α cells. The genomic integration sites of retrovirus vectors were determined in our previous study.[32] Sequences of resulting clones were subjected to a human BLAST search at http://blast.ncbi.nlm.nih.gov/Blast.cgi and analyzed as described previously.[32]

Enzyme-linked immunosorbent assay

Supernatants from duplicate wells of the target 3T3/CD19 cell and effector CD19-CAR T-cell co-culture (10^{5} cells each) were harvested after 48-h incubation. Supernatant human IFN-γ levels were measured using a human IFN-γ enzyme-linked immunosorbent assay kit (Biolegend).

Cytotoxicity assay

Cell lytic activity was examined using calcein acetoxymethyl ester (Calcein-AM) (Dojindo, Kumamoto, Japan) cytotoxicity assays.[33] Calcein-AM-labeled Raji cells and K562 target cells (10^{4} each) were co-cultured with increasing numbers of effector CD19-CAR T-cells. After 4-h incubation, supernatants were harvested and transferred into 96-well plates. Sample fluorescence was read by Fluoroskan Ascent FL (Thermo Fisher Scientific, Waltham, MA, USA). The percentage of lysed cells was calculated with the same formula used for ^{51}Cr release assays.[34]

Mouse tumor model

Balb/c Rag2$^{-/-}$γc$^{-/-}$ (10–12-weeks old) immunodeficient mice[35–37] were intravenously injected with 5×10^{4} Raji/Luc cells on day 0. Mice were intravenously injected with 10^{7} CD19-CAR T-cells alone on day 3 or T-cells in combination with either intraperitoneal injection of an anti-PD-1 antibody (Clone J116; Bio-XCell, West Lebanon, NH, USA)[38] at 250 μg per mouse (on days 3, 10 and 17) or intramuscular injection of AAV-IL-7 (10^{11} vg per body) on day 3.[19] Bioluminescence imaging was performed and analyzed using an IVIS imaging system with the Living Image software (PerkinElmer, Waltham, MA, USA) as described previously.[15] All mouse experiments were carried out humanely following approval from the Institutional Animal Experiment Committee of Jichi Medical University.

Statistical analysis

The Student's *t*-test was used to evaluate differences in experiments. GraphPad Prism 5 (GraphPad Software, San Diego, CA, USA) was used to analyze statistical calculations. A value of $P < 0.05$ was considered statistically significant.

Nucleotide sequence accession numbers

Reported nucleotide sequence data are available from the DDBJ/EMBL/GenBank database under accession nos. AB917147–AB917152 and LC002285–LC002289.

CONFLICT OF INTEREST

The authors declare no conflict of interest.

ACKNOWLEDGEMENTS

We thank Miyoko Mitsu and Satomi Fujiwara for the AAV preparations. This work was supported in part by a Grant-in-Aid for Scientific Research (Nos. 22700923 and 24390247), a JMU Graduate Student Start-Up Grant for Young Investigators to N Iwase and the MEXT-Supported Program for the Strategic Research Foundation at Private Universities, 2013–2017. We thank Dr M Ito (Central Institute for Experimental Animals) for providing Balb/c Rag2$^{-/-}$γc$^{-/-}$ mice. We also thank JMU Core Center of Research Apparatus for assistance with flow cytometry. This publication was subsidized by JKA through its promotion funds from KEIRIN RACE.

REFERENCES

1 Davila ML, Brentjens R, Wang X, Riviere I, Sadelain M. How do CARs work?: Early insights from recent clinical studies targeting CD19. *Oncoimmunology* 2012; **1**: 1577–1583.
2 Kochenderfer JN, Rosenberg SA. Treating B-cell cancer with T cells expressing anti-CD19 chimeric antigen receptors. *Nat Rev Clin Oncol* 2013; **10**: 267–276.
3 Kawakami K. Tol2: a versatile gene transfer vector in vertebrates. *Genome Biol* 2007; **8**(Suppl 1): S7.
4 Yagita K, Yamanaka I, Emoto N, Kawakami K, Shimada S. Real-time monitoring of circadian clock oscillations in primary cultures of mammalian cells using Tol2 transposon-mediated gene transfer strategy. *BMC Biotechnol* 2010; **10**: 3.
5 Kawakami K, Noda T. Transposition of the Tol2 element, an Ac-like element from the Japanese medaka fish Oryzias latipes, in mouse embryonic stem cells. *Genetics* 2004; **166**: 895–899.
6 Suster ML, Sumiyama K, Kawakami K. Transposon-mediated BAC transgenesis in zebrafish and mice. *BMC Genomics* 2009; **10**: 477.
7 Urasaki A, Morvan G, Kawakami K. Functional dissection of the Tol2 transposable element identified the minimal cis-sequence and a highly repetitive sequence in the subterminal region essential for transposition. *Genetics* 2006; **174**: 639–649.
8 Rostovskaya M, Fu J, Obst M, Baer I, Weidlich S, Wang H *et al.* Transposon-mediated BAC transgenesis in human ES cells. *Nucleic Acids Res* 2012; **40**: e150.

9 Grabundzija I, Irgang M, Mates L, Belay E, Matrai J, Gogol-Doring A *et al.* Comparative analysis of transposable element vector systems in human cells. *Mol Ther* 2010; **18**: 1200–1209.
10 Manuri PV, Wilson MH, Maiti SN, Mi T, Singh H, Olivares S *et al.* piggyBac transposon/transposase system to generate CD19-specific T cells for the treatment of B-lineage malignancies. *Hum Gene Ther* 2010; **21**: 427–437.
11 Singh H, Manuri PR, Olivares S, Dara N, Dawson MJ, Huls H *et al.* Redirecting specificity of T-cell populations for CD19 using the Sleeping Beauty system. *Cancer Res* 2008; **68**: 2961–2971.
12 Kebriaei P, Huls H, Jena B, Munsell M, Jackson R, Lee DA *et al.* Infusing CD19-directed T cells to augment disease control in patients undergoing autologous hematopoietic stem-cell transplantation for advanced B-lymphoid malignancies. *Hum Gene Ther* 2012; **23**: 444–450.
13 Singh H, Figliola MJ, Dawson MJ, Huls H, Olivares S, Switzer K *et al.* Reprogramming CD19-specific T cells with IL-21 signaling can improve adoptive immunotherapy of B-lineage malignancies. *Cancer Res* 2011; **71**: 3516–3527.
14 Saito S, Nakazawa Y, Sueki A, Matsuda K, Tanaka M, Yanagisawa R *et al.* Anti-leukemic potency of piggyBac-mediated CD19-specific T cells against refractory Philadelphia chromosome-positive acute lymphoblastic leukemia. *Cytotherapy* 2014; **16**: 1257–1269.
15 Tsukahara T, Ohmine K, Yamamoto C, Uchibori R, Ido H, Teruya T *et al.* CD19 target-engineered T-cells accumulate at tumor lesions in human B-cell lymphoma xenograft mouse models. *Biochem Biophys Res Commun* 2013; **438**: 84–89.
16 Okazaki T, Chikuma S, Iwai Y, Fagarasan S, Honjo T. A rheostat for immune responses: the unique properties of PD-1 and their advantages for clinical application. *Nat Immunol* 2013; **14**: 1212–1218.
17 John LB, Devaud C, Duong CP, Yong CS, Beavis PA, Haynes NM *et al.* Anti-PD-1 antibody therapy potently enhances the eradication of established tumors by gene-modified T cells. *Clin Cancer Res* 2013; **19**: 5636–5646.
18 Lundstrom W, Fewkes NM, Mackall CL. IL-7 in human health and disease. *Semin Immunol* 2012; **24**: 218–224.
19 Xin KQ, Urabe M, Yang J, Nomiyama K, Mizukami H, Hamajima K *et al.* A novel recombinant adeno-associated virus vaccine induces a long-term humoral immune response to human immunodeficiency virus. *Hum Gene Ther* 2001; **12**: 1047–1061.
20 Maiti SN, Huls H, Singh H, Dawson M, Figliola M, Olivares S *et al.* Sleeping beauty system to redirect T-cell specificity for human applications. *J Immunother* 2013; **36**: 112–123.
21 Peng PD, Cohen CJ, Yang S, Hsu C, Jones S, Zhao Y *et al.* Efficient nonviral Sleeping Beauty transposon-based TCR gene transfer to peripheral blood lymphocytes confers antigen-specific antitumor reactivity. *Gene Therapy* 2009; **16**: 1042–1049.
22 Jin Z, Maiti S, Huls H, Singh H, Olivares S, Mates L *et al.* The hyperactive Sleeping Beauty transposase SB100X improves the genetic modification of T cells to express a chimeric antigen receptor. *Gene Therapy* 2011; **18**: 849–856.
23 Hacein-Bey-Abina S, Von Kalle C, Schmidt M, McCormack MP, Wulffraat N, Leboulch P *et al.* LMO2-associated clonal T cell proliferation in two patients after gene therapy for SCID-X1. *Science* 2003; **302**: 415–419.
24 Scholler J, Brady TL, Binder-Scholl G, Hwang WT, Plesa G, Hege KM *et al.* Decade-long safety and function of retroviral-modified chimeric antigen receptor T cells. *Sci Transl Med* 2012; **4**: 132ra53.
25 Huang X, Guo H, Tammana S, Jung YC, Mellgren E, Bassi P *et al.* Gene transfer efficiency and genome-wide integration profiling of Sleeping Beauty, Tol2, and piggyBac transposons in human primary T cells. *Mol Ther* 2010; **18**: 1803–1813.
26 Kogure K, Urabe M, Mizukami H, Kume A, Sato Y, Monahan J *et al.* Targeted integration of foreign DNA into a defined locus on chromosome 19 in K562 cells using AAV-derived components. *Int J Hematol* 2001; **73**: 469–475.
27 Sadelain M, Papapetrou EP, Bushman FD. Safe harbours for the integration of new DNA in the human genome. *Nat Rev Cancer* 2012; **12**: 51–58.
28 Ammar I, Gogol-Doring A, Miskey C, Chen W, Cathomen T, Izsvak Z *et al.* Retargeting transposon insertions by the adeno-associated virus Rep protein. *Nucleic Acids Res* 2012; **40**: 6693–6712.
29 Brentjens RJ, Santos E, Nikhamin Y, Yeh R, Matsushita M, La Perle K *et al.* Genetically targeted T cells eradicate systemic acute lymphoblastic leukemia xenografts. *Clin Cancer Res* 2007; **13**(Pt 1): 5426–5435.
30 Yagi H, Ogura T, Mizukami H, Urabe M, Hamada H, Yoshikawa H *et al.* Complete restoration of phenylalanine oxidation in phenylketonuria mouse by a self-complementary adeno-associated virus vector. *J Gene Med* 2011; **13**: 114–122.
31 Latouche JB, Sadelain M. Induction of human cytotoxic T lymphocytes by artificial antigen-presenting cells. *Nat Biotechnol* 2000; **18**: 405–409.
32 Tsukahara T, Agawa H, Matsumoto S, Matsuda M, Ueno S, Yamashita Y *et al.* Murine leukemia virus vector integration favors promoter regions and regional hot spots in a human T-cell line. *Biochem Biophys Res Commun* 2006; **345**: 1099–1107.
33 Neri S, Mariani E, Meneghetti A, Cattini L, Facchini A. Calcein-acetyoxymethyl cytotoxicity assay: standardization of a method allowing additional analyses on recovered effector cells and supernatants. *Clin Diagn Lab Immunol* 2001; **8**: 1131–1135.
34 Kannagi M, Sugamura K, Sato H, Okochi K, Uchino H, Hinuma Y. Establishment of human cytotoxic T cell lines specific for human adult T cell leukemia virus-bearing cells. *J Immunol* 1983; **130**: 2942–2946.
35 Ohbo K, Suda T, Hashiyama M, Mantani A, Ikebe M, Miyakawa K *et al.* Modulation of hematopoiesis in mice with a truncated mutant of the interleukin-2 receptor gamma chain. *Blood* 1996; **87**: 956–967.
36 Ohteki T, Fukao T, Suzue K, Maki C, Ito M, Nakamura M *et al.* Interleukin 12-dependent interferon gamma production by CD8alpha+ lymphoid dendritic cells. *J Exp Med* 1999; **189**: 1981–1986.
37 Shinkai Y, Rathbun G, Lam KP, Oltz EM, Stewart V, Mendelsohn M *et al.* RAG-2-deficient mice lack mature lymphocytes owing to inability to initiate V(D)J rearrangement. *Cell* 1992; **68**: 855–867.
38 Wang C, Yi T, Qin L, Maldonado RA, von Andrian UH, Kulkarni S *et al.* Rapamycin-treated human endothelial cells preferentially activate allogeneic regulatory T cells. *J Clin Invest* 2013; **123**: 1677–1693.

Supplementary Information accompanies this paper on Gene Therapy website (http://www.nature.com/gt)

Cancer Science
Japanese Cancer Association JCA
Open Access

Novel anti-tumor mechanism of galanin receptor type 2 in head and neck squamous cell carcinoma cells

Takayuki Uehara,[1,2,3] Takeharu Kanazawa,[3,6] Hiroaki Mizukami,[2,6] Ryosuke Uchibori,[2] Tomonori Tsukahara,[2] Masashi Urabe,[2] Akihiro Kume,[2] Kiyoshi Misawa,[4] Thomas E. Carey,[5] Mikio Suzuki,[1] Keiichi Ichimura[3] and Keiya Ozawa[2,6]

[1]Department of Otorhinolaryngology, Head and Neck Surgery, Graduate School of Medicine, University of the Ryukyus, Nishihara; [2]Division of Genetic Therapeutics, Center for Molecular Medicine, Jichi Medical University, Shimotsuke; [3]Department of Otolaryngology, Head and Neck Surgery, Jichi Medical University School of Medicine, Shimotsuke; [4]Department of Otolaryngology, Head and Neck Surgery, Hamamatsu University School of Medicine, Hamamatsu, Japan; [5]Laboratory of Head and Neck Center Biology, Department of Otolaryngology, Head and Neck Surgery, The University of Michigan, Ann Arbor, Michigan, USA

Key words

Adeno-associated virus vector, Bim, extracellular signal-regulated kinases 1/2, galanin receptor, head and neck squamous cell carcinoma

Correspondence

Takeharu Kanazawa, Department of Otolaryngology, Head and Neck Surgery, Jichi Medical University School of Medicine, 3311-1 Yakushiji, Shimotsuke 329-0498, Japan.
Tel: 0285-58-7381; Fax: 0285-44-5547;
E-mail: kanatake@omiya.jichi.ac.jp

[6]These three authors made an equal contribution towards the conduct and reporting of this study.

Funding information

Ministry of Education, Culture, Sports, Science, and Technology of Japan (22591916, 23592539)

Received June 25, 2013; Revised October 23, 2013; Accepted October 27, 2013

Cancer Sci **105** (2014) 72–80

doi: 10.1111/cas.12315

Galanin and its receptors, GALR1 and GALR2, are known tumor suppressors and potential therapeutic targets in head and neck squamous cell carcinoma (HNSCC). Previously, we demonstrated that, in GALR1-expressing HNSCC cells, the addition of galanin suppressed tumor proliferation via upregulation of ERK1/2 and cyclin-dependent kinase inhibitors, whereas, in GALR2-expressing cells, the addition of galanin not only suppressed proliferation, but also induced apoptosis. In this study, we first transduced HEp-2 and KB cell lines using a recombinant adeno-associated virus (rAAV)-green fluorescent protein (GFP) vector and confirmed a high GFP expression rate (>90%) in both cell lines at the standard vector dose. Next, we demonstrated that GALR2 expression in the presence of galanin suppressed cell viability to 40–60% after 72 h in both cell lines. Additionally, the annexin V-positive rate and sub-G0/G1 phase population were significantly elevated in HEp-2 cells (mock *vs* GALR2: 12.3 *vs* 25.0% ($P < 0.01$) and 9.1 *vs* 32.0% ($P < 0.05$), respectively) after 48 h. These changes were also observed in KB cells, although to a lesser extent. Furthermore, in HEp-2 cells, GALR2-mediated apoptosis was caspase-independent, involving downregulation of ERK1/2, followed by induction of the pro-apoptotic Bcl-2 protein, Bim. These results illustrate that transient GALR2 expression in the presence of galanin induces apoptosis via diverse pathways and serves as a platform for suicide gene therapy against HNSCC.

Head and neck squamous cell carcinoma (HNSCC) is diagnosed in more than 500 000 patients worldwide each year, accounting for 5% of all malignancies.[1,2] Despite multidisciplinary therapy, the prognosis of patients with advanced HNSCC has remained poor over several decades.[3] Thus, the invention of new therapeutic approaches against HNSCC, such as gene therapy and molecular targeted therapies has received much attention.[4–7] However, these novel treatments remain inadequate, because various signal transduction systems are defective in typical HNSCC, and little therapeutic effect is achieved by therapies targeting single mechanisms. Thus, there is a need to develop an effective drug delivery system and a novel molecular targeted therapy with multiple therapeutic targets.

In general, tyrosine kinase receptors and cytokine receptors, and their signaling pathways are important in carcinogenesis[5,8] and they have been analyzed as molecular targets and prognostic factors in HNSCC. However, the roles of G-protein–coupled receptors (GPCRs), which are important signaling molecules, are not fully understood. GPCRs control various signaling pathways in all tissues of the body, and approximately 30% of all current pharmaceuticals exert their therapeutic effects by interacting with GPCRs. Therefore, the field of GPCRs holds promise for further drug discovery and therapeutic development.[9]

Previously, we investigated the function and signal transduction of galanin receptors, which are representative GPCRs in HNSCC.[10,11] Galanin is a 30-amino acid peptide, which has three specific receptors (GALR1–3). Galanin and its receptors are mainly expressed in the central and peripheral nervous systems and function in neurotransmission.[12–14] Recently, galanin has been shown to regulate cell proliferation and survival in many tumors.[15–17] With the development of functional analysis methods for each receptor, it became clear that GALR1 and GALR2 are likely to act as tumor suppressors. Our previous study showed that activation of the GALR1 signaling pathway suppressed tumor cell proliferation via phosphorylation of ERK1/2, and involves upregulation of the cyclin-dependent kinase inhibitors in HNSCC.[10,18] Other studies showed that GALR1 inhibits proliferation by inactivat-

ing the mitogen-activated protein kinase (MAPK) pathway in oral carcinoma.[19] Moreover, activation of the GALR2 signaling pathway suppresses tumor cell growth through induction of apoptosis in some tumors, including HNSCC.[11,20,21] The cytotoxic effects of the GALR2 signaling pathway are partially mediated by dephosphorylation of Akt and the Bcl-2 protein, Bad, in PC12 cells, a pheochromocytoma cell line.[21]

However, further analysis is required with respect to prognostic factors in HNSCC, applications of molecular targeted therapy, and clinical applications of gene therapy. The adeno-associated (AAV) vector is a promising system in gene therapy, holding various benefits, such as a lack of pathogenicity, low immunogenicity, long-term transgene expression, and broad tissue-specificity.[22,23] To date, AAV vectors have been used in clinical trials for the treatment of various diseases, such as Parkinson's disease, hemophilia B, and inherited retinal disorders.[24–27] Additionally, it is thought to be applicable to suicide-gene therapy against various cancers, including HNSCC.[28–30] rAAV-galanin is currently clinically applied in the suppression of limbic seizure activity,[31] and this vector is suitable for use in the galanin–GALR system. Given this background, we set out to evaluate the effects of GALR expression on apoptosis and analyzed the associated mechanism of action using HNSCC cells.

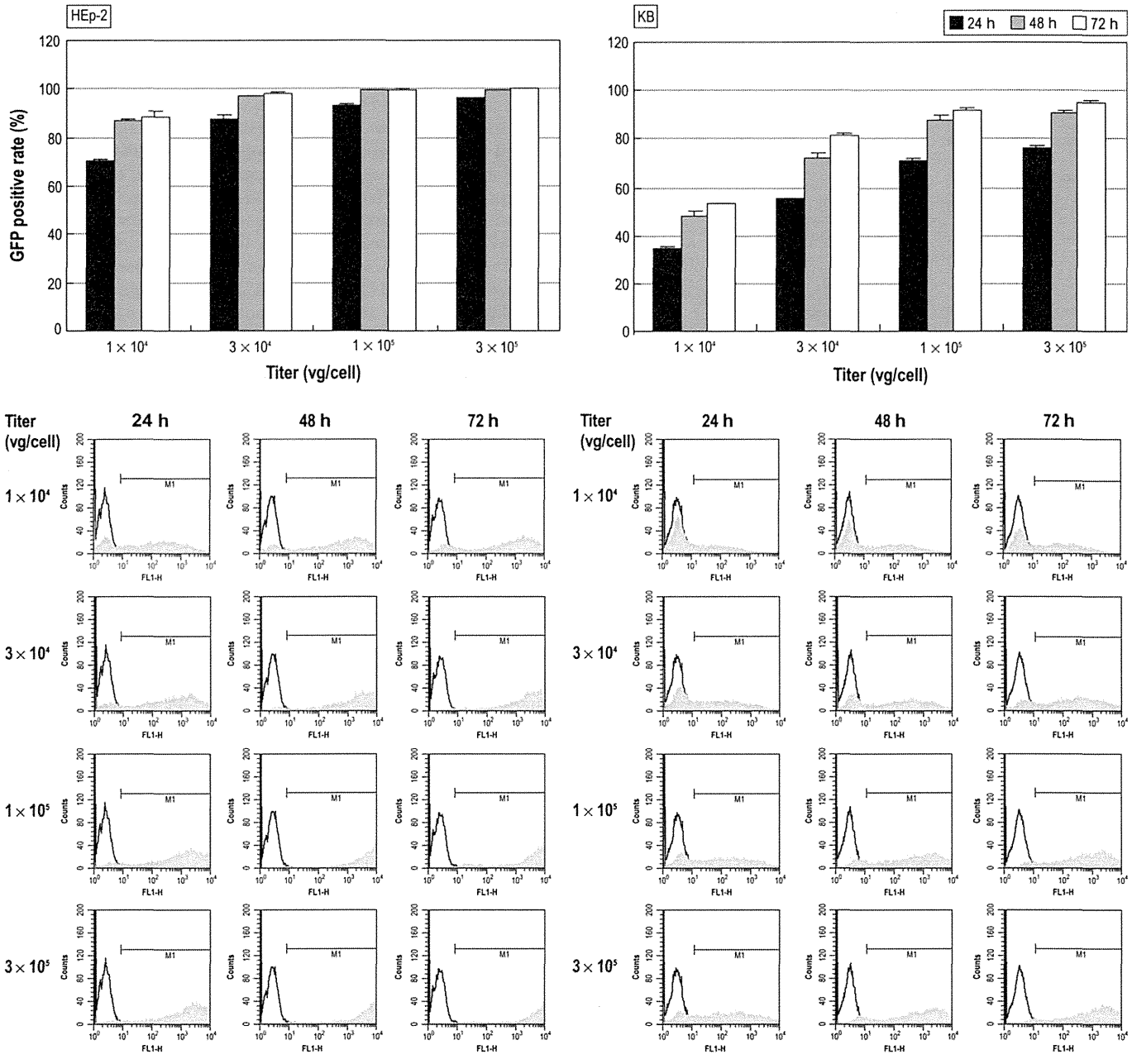

Fig. 1. Transduction efficiency using recombinant adeno-associated virus (rAAV)-enhanced green fluorescent protein (EGFP) in head and neck squamous cell carcinoma (HNSCC) cell lines. HEp-2 and KB cells were transduced by AAV-EGFP at various vector doses. *Upper*: GFP-positive cell rate under vector dose-dependent and time-course conditions in each cell line are indicated. *Lower*: Raw data expressing GFP intensity as a measure of gene expression.

Material and Methods

Cell culture and reagents. Human laryngeal carcinoma cell line HEp-2 and human oral carcinoma cell line KB were purchased from American Type Culture Collection (Manassas, VA, USA). Cells were cultured in αMEM (Gibco, Grand Island, NY, USA) supplemented with 10% heat-inactivated fetal bovine serum, 100 U/mL penicillin, and 100 μg/mL streptomycin. Human galanin was obtained from ANASPEC (San Jose, CA, USA), PD98059 and staurosporine from Wako (Osaka, Japan), and z-VAD-fmk from Promega (Madison, WI, USA). Although KB cells were originally thought to be derived from an epidermal carcinoma of the mouth, HeLa cell contamination was found thereafter through isoenzyme and other analyses (http://www.atcc.org/Products/All/CCL-17.aspx). Therefore, KB cells may not be a pure HNSCC cell line. However, we used both cell lines to understand the universal function of GALR2, rather than its cell-specific function.

Plasmid and rAAV vector production. The GALR1HA-Ires-GFP and GALR2HA-Ires-GFP fragments were obtained from our previous experiments.[10] The sequences were subcloned into the pAAV-MCS vector (Agilent technologies, Palo Alto, CA, USA).

To produce recombinant AAV vectors, we used an AAV helper-free system (Agilent technologies). Each pAAV vector, pAAV-RC, and the pHelper plasmid were cotransfected into subconfluent HEK293 cells by the calcium phosphate precipitation method or by polyethylenimine. After 72-h incubation, cells were harvested and lysed using three freeze-thaw cycles. The crude viral lysate was purified by two rounds of CsCl density-gradient ultracentrifugation. The titer of rAAV vectors was subsequently determined by quantitative PCR analysis.

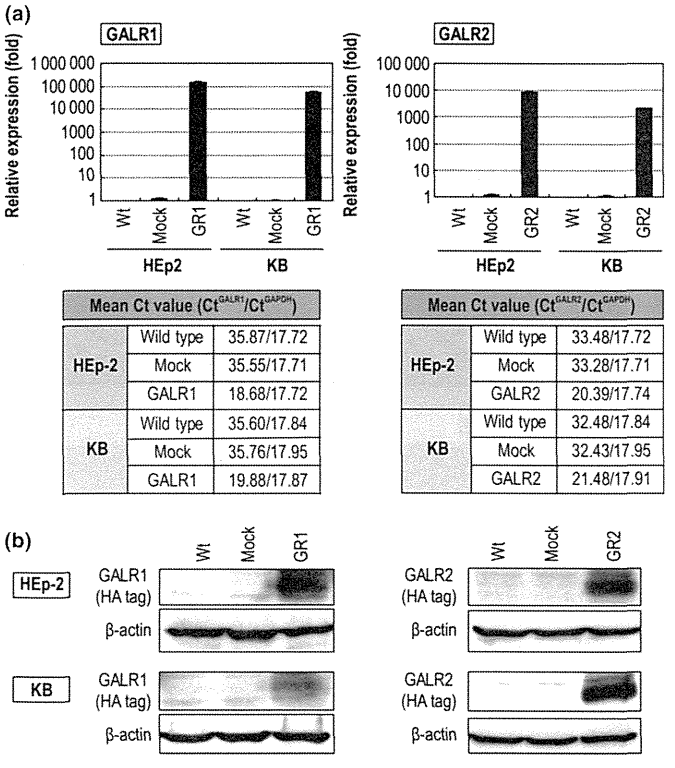

Fig. 2. Expression of GALR1 and GALR2 using individual recombinant AAV vectors in head and neck squamous cell carcinoma (HNSCC) cells. (a) Quantitative RT-PCR was performed to measure GALR1 and GALR2 expression in wild type (Wt) or HNSCC cells transduced by each of the rAAV vectors. (b) Western blot results showing exogenous GALR1 and GALR2 expression in Wt or HNSCC cells transduced by each of the rAAV vectors, as detected by an HA-antibody.

Quantitative RT-PCR. Total RNA was isolated using an RNeasy mini kit (Qiagen, Valencia, CA, USA). Reverse transcription was performed using a High Capacity cDNA Reverse Transcription Kit (Applied Biosystems, Foster City, CA, USA) according to the manufacturer's protocol. cDNA was amplified using TaqMan Expression Assays (Applied Biosystems): GalR1 (Hs00175668 m1), GalR2 (Hs00605839 m1), and GAPDH (Hs99999905 m1). The PCR conditions were as follows: 50°C for 2 min, 95°C for 10 min, and 40 cycles each consisting of 95°C for 15 s and 60°C for 1 min. The expression levels of the target genes were analyzed using the comparative C_t method, and GAPDH was used as a control gene.

Immunoblotting. Cells were lysed in a buffer containing 62.5 mM Tris-HCl (pH6.8), 2% SDS, 10% glycerol, 6% mercaptoethanol, and 0.01% bromophenol blue. To detect GALRs expression, cell lysates were treated with N-Glycosidase F (New England BioLabs, Beverley, MA, USA) without boiling, as described previously.[10,11] Mitochondrial and cytosolic fractions were obtained using Mitochondrial Isolation Kit (ThermoFisher Scientific, Logan, UT, USA).

Samples were gel electrophoresed and transferred to polyvinylidene difluoride membranes, which were probed with specific antibodies. Mouse monoclonal antibodies to hemagglutinin (HA)-tag, phospho-Bad (Ser112), and β-actin, rabbit monoclonal antibodies to p44/42 MAPK (Erk1/2), phospho-p44/42 (Thr202/Tyr204), Akt, phospho-Akt, caspase-3, cleaved caspase-3, Bax, Bcl-2, Bcl-xL, Mcl-1, Bim, Bad, survivin, antibodies to Cox IV and XIAP, polyclonal antibodies to AIF, Endonuclease G, Bit1, HtrA2 and cytochrome c were purchased from Cell Signaling Technology (Beverly, MA, USA). Bands were visualized using an Enhanced Chemiluminescence Kit (GE Healthcare, Buckinghamshire, UK) and an ImageQuant LAS 4000 (Fujifilm, Tokyo, Japan).

Immunocytochemistry. Cells were seeded onto coverslips and incubated overnight, and transduced with each recombinant AAV vector. After 48 h of incubation, cells were fixed, and stained with mouse monoclonal anti-HA-tag antibody (Cell Signaling). Subsequently, cells were stained with Alexa Fluor 555-labeled goat anti-mouse IgG (Cell Signaling) and the nuclei counterstained with DAPI. Furthermore, to determine the transport potential of HA-tagged GALRs proteins to the cytoplasmic membrane, HEp-2 cells stably expressing these proteins were established by transfecting the AAV plasmid into HEp-2 cells using Lipofectamine (Invitrogen, Carlsbad, CA, USA). Green fluorescent protein-positive cells were selected by flow cytometry using a FACS Vantage SE at 4 weeks after transfection (BD Biosciences, San Diego, CA, USA). Exogenous GALR1 or GALR2 were localized using a BIOREVO BZ-9000 microscope (Keyence, Osaka, Japan) and an Olympus FV-500 Confocal Microscope (Olympus Corporation, Tokyo, Japan).

Cell viability assay. The effect of activation of the GALR signaling pathways on cell viability was examined using WST-1 (Roche Diagnostics, East Sussex, UK). Cells were seeded in a 96-well microculture plate, incubated overnight, and then cultured in serum-free media (SFM) containing 0.1% bovine serum albumin for 2 h. Subsequently, cells were exposed to the individual rAAV vectors and galanin for 24–72 h. WST-1 reagent was added for the last 1–2 h of the incubation, and the absorbance at 450 nm was measured

using a Spectra Max 190 microplate reader (Molecular Devices, Sunnyvale, CA, USA).

Apoptosis and cell cycle analysis. Apoptotic cells were detected by staining with phycoerythrin (PE)-conjugated annexin V protein (BD Bioscience, San Jose, CA, USA) and flow cytometry. Cell cycle analysis was performed with the CycleTEST PLUS DNA Reagent Kit (BD Biosciences) and flow cytometry. Apoptosis-induced DNA fragmentation was measured for the sub-G0/G1 cell cycle phase populations.

Statistical analysis. Statistical analysis was performed using Student's *t*-test and Kruskal–Wallis test.

Results

Transduction efficiency of HNSCC cell lines using rAAV-EGFP. To determine transduction efficiency in HNSCC cell lines using rAAV vectors, HEp-2 and KB cells were infected with a rAAV-EGFP vector at various vector doses. After incubation for 24–72 h, GFP-positive cells were counted by flow cytometry. We confirmed a high GFP expression (>90%) in both HNSCC cell lines transduced by vector doses above 1×10^5 vector genomes (vg)/cell for 48 h (Fig. 1). Consequently, a titer of 1×10^5 vg/cell was used as standard vector dose.

GALR gene expression after transduction of rAAV-GALR vectors. We determined both the endogenous and exogenous mRNA expression levels of each GALR gene in HEp-2 and KB cells transduced by rAAV-GALR1 or rAAV-GALR2 by quantitative RT-PCR. After 48 h of transduction, elevated mRNA expression levels of exogenous GALR1 and GALR2 were observed in both cell lines (Fig. 2a).

The expression levels of exogenous GALR1 and GALR2 proteins were also assessed by western blot analysis and immunocytochemistry, using a mouse monoclonal anti-HA tag antibody, and confirmed robust expression of GALR1 and GALR2 proteins (Figs 2b,3). Immunofluorescence revealed that GFP-positive cells showed exogenous expression of GALRs, which was localized to both the cytoplasm and plasma membrane in cells transiently transduced with AAV vectors (Fig. 3a). However, in stable GALRs-expressing HEp-2 cells, exogenous GALRs located only to the plasma membrane (Fig. 3b). These results suggested that transient-transduction impelled movement of a large quantity of these proteins to the cytoplasm, although these proteins themselves have the potential to be transported to the plasma membrane, as expected for a G protein-coupled receptor.

Co-administration of rAAV-GALR2 and galanin inhibits cell proliferation and induces apoptosis. We examined the ability of each GALR signaling pathway to inhibit HNSCC growth. Culture of cells in the presence of both rAAV-GALR2 and varying doses of galanin in SFM for 24–72 h resulted in cell growth suppression in a time- and dose-dependent manner in both HNSCC lines, as assessed by WST-1 assay. After 72 h of stimulation, the cell growth rate was significantly decreased to 40% in HEp-2 and 60% in KB cells (Fig. 4a). In contrast,

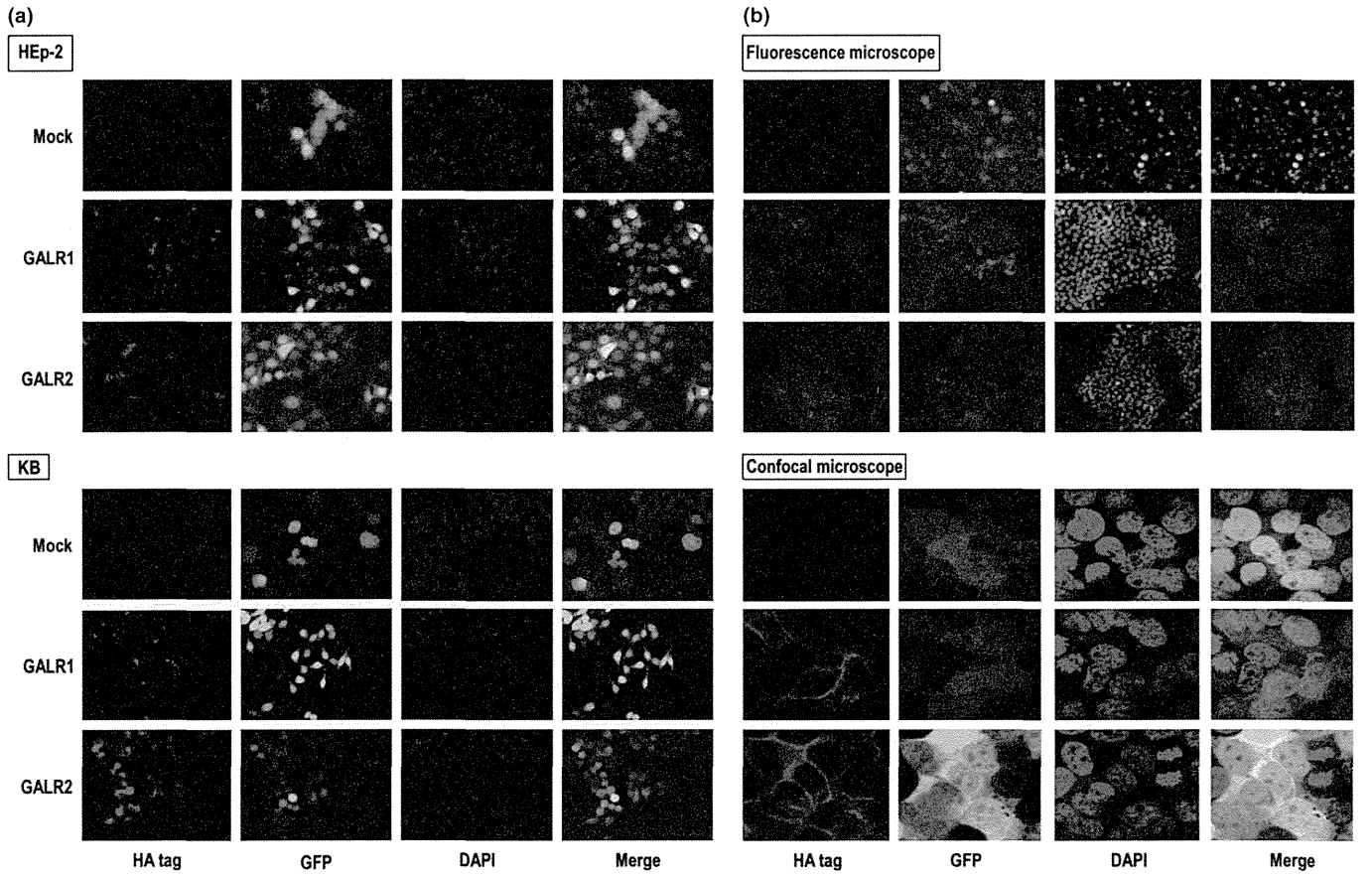

Fig. 3. (a) Exogenous GALR1 and GALR2 localization in head and neck squamous cell carcinoma (HNSCC) cells transiently transduced with each of the recombinant adeno-associated virus (rAAV) vectors. (b) Exogenous GALR1 and GALR2 localization in HEp-2 cells stably transfected with each of the AAV plasmids. Images show cells stained with the anti-HA antibody (left-most), green fluorescent protein (GFP) (second from the left), DAPI (4′6′-diamidino-2-phenylindole dihydrochloride) (second from the right), and merged images (right-most).

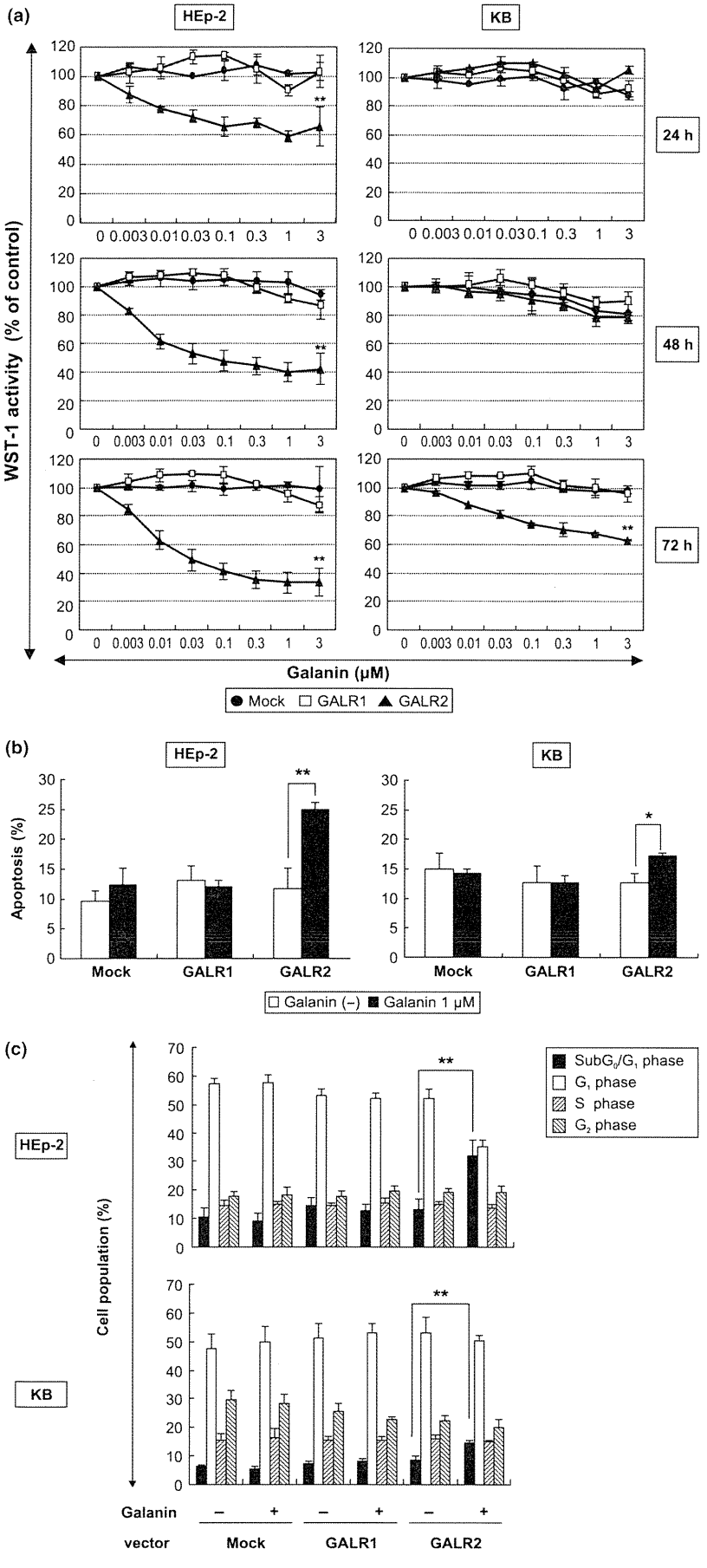

Fig. 4. Co-administration of galanin and recombinant adeno-associated virus (rAAV)-GALR2 during cell culture inhibited cell proliferation and induced cell death in head and neck squamous cell carcinoma (HNSCC) cells. (a) Inhibitory effects of galanin on growth of HNSCC cells transduced with the respective rAAV vectors. (b) Flow cytometric analysis of cell apoptosis using the annexin V. (c) Cell cycle analysis by flow cytometry. $*P < 0.05$; $**P < 0.01$.

co-administration of rAAV-GALR1 and galanin did not affect cell proliferation in either cell line (Fig. 4a).

The ability of GALR signaling to induce apoptosis was assessed by measuring annexin V staining in both cell lines. Co-treatment of cells with rAAV-GALR2 and galanin (1 μM) for 48 h significantly induced apoptosis in 25% of HEp-2 cells, and less markedly induced apoptosis in 16% of KB cells (Fig. 4b).

Furthermore, changes in the cell cycle distribution after activation of either GALR pathway were evaluated by flow cytometry. Co-administration of rAAV-GALR2 vector and galanin (1 μM) for 48 h significantly increased the sub-G0/G1 phase population, to 32% in HEp-2, and to 16.6% in KB cells (Fig. 4c), suggesting that DNA fragmentation was induced by activation of the GALR2 signaling pathway, along with apoptosis. No other effects on cell cycle distribution were observed (Fig. 4c). Additionally, GALR1 activation had no effects on induction of apoptosis or cell cycle distribution (Fig. 4b,c).

Stimulation of GALR2 signaling downregulates ERK1/2, and upregulates Bim. As the GALR2-mediated cytotoxic effects were mainly due to apoptosis induction, we examined whether stimulation of the GALR2 signaling pathway affected the phosphorylation states of ERK1/2 and Akt by immunoblotting. Sustained dephosphorylation of ERK1/2 was induced by stimulation of GALR2 signaling in both HNSCC cell lines (Fig. 5a), but no effect on Akt phosphorylation was observed (Fig. 5b).

Moreover, we examined the influence of the pathway on key apoptosis regulators, viz., the Bcl-2 protein and inhibitor of apoptosis protein (IAP) families. The proapoptotic "BH-3–only" Bcl-2 protein Bim was upregulated by activation of GALR2 signaling in HEp-2, but not in KB cells (Fig. 5a,c). No other apoptosis-related proteins investigated were affected by GALR2 activation in either cell line (Fig. 5c). Additionally, activation of GALR1 signaling did not affect the phosphorylation state of ERK or the other apoptotic regulators (Fig. 5c).

PD98059 inhibits cell proliferation and induces apoptosis via inactivation of the MEK/ERK pathway in HNSCC cells. To determine whether dephosphorylation of ERK1/2 results in cell growth inhibition and apoptosis induction in HNSCC cells, we examined the reproducibility of GALR2-mediated cytotoxicity using a specific ERK (MEK1) inhibitor, PD98059. As expected, dephosphorylation of ERK1/2 was induced by treatment of both HNSCC cell lines with PD98059 at 20–100 μM for 48 h (Fig. 6a). When cells were cultured in SFM in the presence of PD98059 for 48 h, dose-dependent cell growth suppression (Fig. 6b) and significant apoptosis induction (Fig. 6c) were observed; these effects were more marked in HEp-2 cells. In addition, dose-dependent upregulation of Bim was observed in HEp-2, but not in KB cells, after incubation with PD98059 for 48 h (Fig. 6a). Thus, the GALR2-mediated cytotoxic effects involved at least downregulation of ERK1/2, while Bim may play a role in modulation of GALR2-mediated apoptotic sensitivity. However, despite apoptosis induction in KB cells, Bim activation was not observed, suggesting the existence of multiple signaling pathways for apoptosis induction.

GALR2-mediated apoptosis is mainly induced via a caspase-independent pathway. We further investigated the role of the caspase signaling pathway in GALR2-mediated apoptosis by

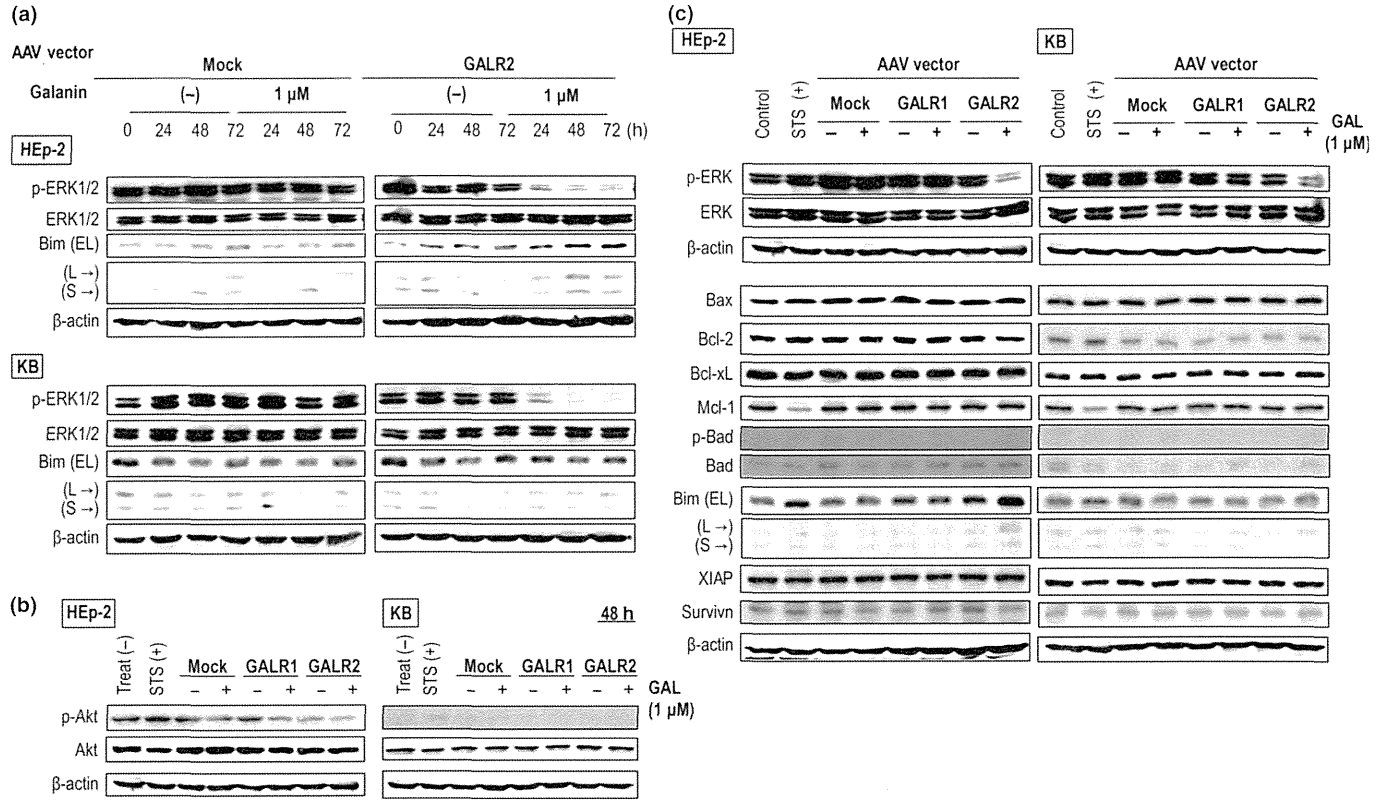

Fig. 5. Immunoblotting analysis of the phosphorylation of ERK1/2 and Akt and regulation of key apoptosis regulators by co-administration of recombinant adeno-associated virus (rAAV)-GALR2 vector and galanin. (a) Effect of galanin on ERK1/2 activation and Bim expression in rAAV-GALR2 vector-transduced head and neck squamous cell carcinoma (HNSCC) cells. (b) Effect of galanin on Akt activation in GALR-transduced HNSCC cells. (c) Effects of treatment of cells with galanin and transduction with individual rAAV vectors on the phosphorylation state of ERK1/2 and expression of proteins belonging to the Bcl-2 or IAP families.

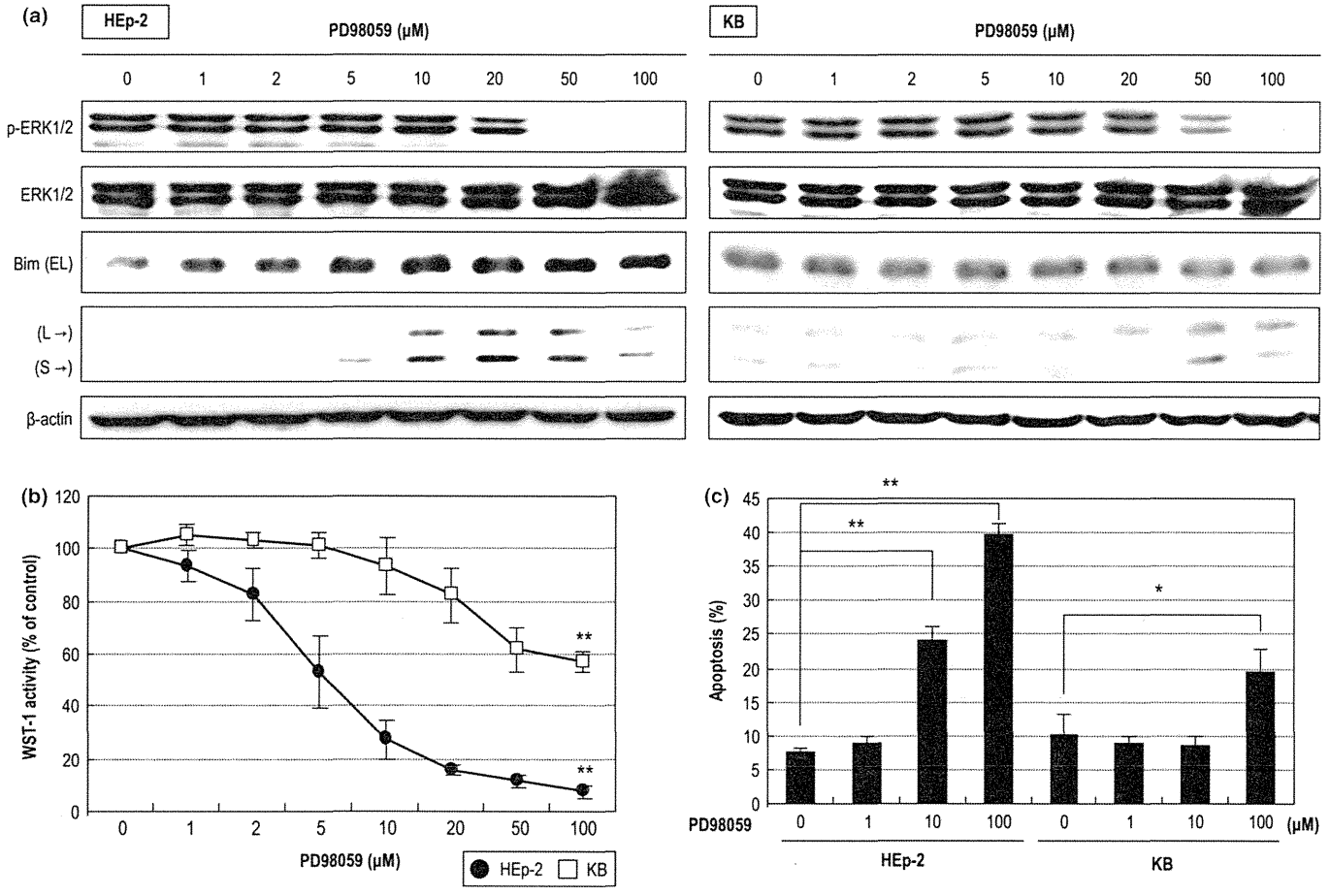

Fig. 6. Effect of the MEK inhibitor PD98059 on head and neck squamous cell carcinoma (HNSCC) cells. (a) Phosphorylation states of ERK1/2 after treatment with PD98059. (b) Effect of PD98059 on proliferation of HNSCC cells. (c) Apoptosis analysis by an Annexin V in HNSCC cells. $*P < 0.05$, $**P < 0.01$.

measuring the cleavage of caspase-3 by immunoblotting. Compared to cells treated with 1 μM staurosporine (STS), minimal cleavage of caspase-3 was observed after stimulation of GALR2 signaling pathway in either HNSCC line (Fig. 7a). Additionally, GALR2-mediated inhibition of cell growth was not abrogated by pretreatment with the pan-caspase inhibitor z-VAD-FMK (50 μM) in HEp-2 cells (Fig. 7b).

We further examined whether activation of mitochondrial apoptosis-related factors were involved in initiating a caspase-independent pathway. Apoptosis inducers, such as apoptosis inducing factor (AIF), endonuclease G, HtrA2, and Bit1, are known to be released from the mitochondria to the cytosol and the nucleus by caspase-independent apoptotic signals. No translocation of these proteins in response to GALR2 activation (Fig. 8) was seen in mitochondrial and cytosolic fractions from transduced HEp-2 cells cultured with/without galanin (1 μM) for 48 h.

Discussion

We previously demonstrated the function of the GALR1 and GALR2 signaling pathways. In HNSCC cell lines, we showed that stably re-expressed GALR1 suppressed tumor cell proliferation via ERK1/2-mediated effects on cyclin-dependent kinase inhibitors, whereas, in GALR2-transduced HNSCC cells, galanin suppressed cell proliferation and induced apoptosis. Thus, we deduced that GALR1 and GALR2 function as tumor suppressors and therefore focused on these proteins as therapeutic targets for HNSCC.

Here, we showed that transduction of GALR2 using rAAV vectors makes HNSCC cells susceptible to galanin-induced growth inhibition and apoptosis; however, we could not show anti-tumor effects of rAAV-mediated GALR1 activation in HNSCC cells. It is unclear why GALR1 and GALR2 have such different effects. We considered that, because of constitutive phosphorylation of ERK1/2 even under serum-free culture conditions in the HNSCC cells used in our experiments, further activation of ERK1/2 by GALR1 activation may not be critical to cell proliferation and survival in these cells.

Although these mechanisms are thought to be partially responsible for tumor cell growth inhibition, the apoptosis induction mechanisms mediated in HNSCC cells by GALR2 activation remain unclear. Our results indicated that downregulation of ERK1/2 is important as a novel apoptotic mechanism triggered by GALR2 activation.

Dephosphorylation of ERK1/2 via stimulation of other GPCRs has previously been reported. Yamada *et al.* reported that angiotensin I type 2 receptor (AT2R) mediated apoptosis followed by dephosphorylation of MAPK in growth factor-supported PC12 cells.[32] Others have reported that inhibition of MAPKs via AT2R was mediated by stimulation of serine/threonine phosphatase 2A (PP2A).[33] It has been reported that phosphotyrosine phosphatase DEP-1/PTPη-dependent dephosphorylation of ERK1/2 is required for inhibition of basic

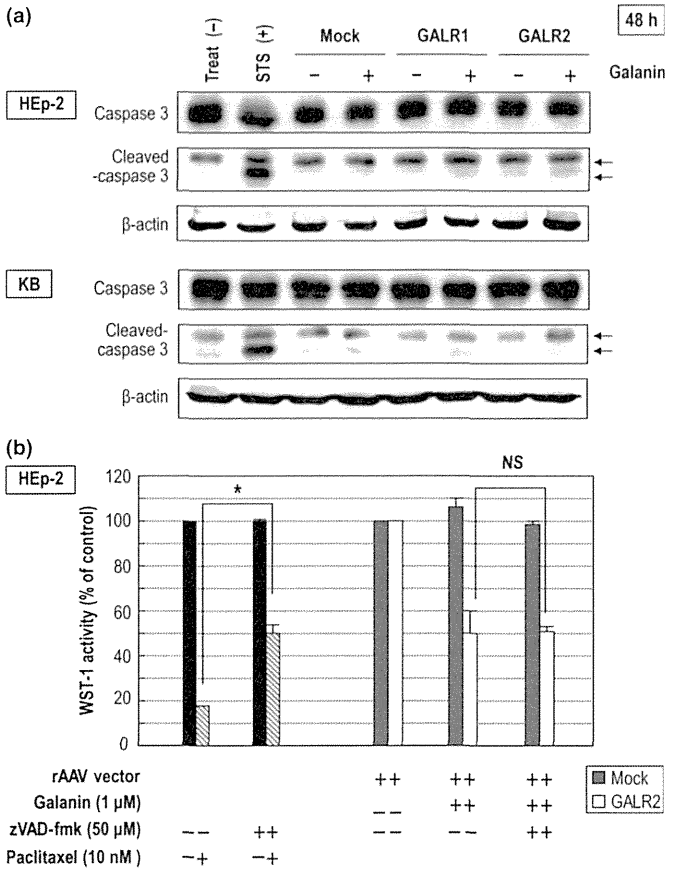

Fig. 7. Effect of galanin on the caspase signaling pathway in recombinant adeno-associated virus (rAAV)-GALR2 vector-transduced head and neck squamous cell carcinoma (HNSCC) cells. (a) Assessment of caspase-3 activation by immunoblotting. Staurosporine (STS; 1 μM) for 3 h was used as a positive control for caspase activation. (b) Effect of a pan-caspase inhibitor (z-VAD-fmk) on GALR2-mediated cytotoxic effects in HEp-2 cells. As positive control, to indicate the inhibitory effect of z-VAD-fmk, we used cells exposed to paclitaxel (10 nM) for 48 h.

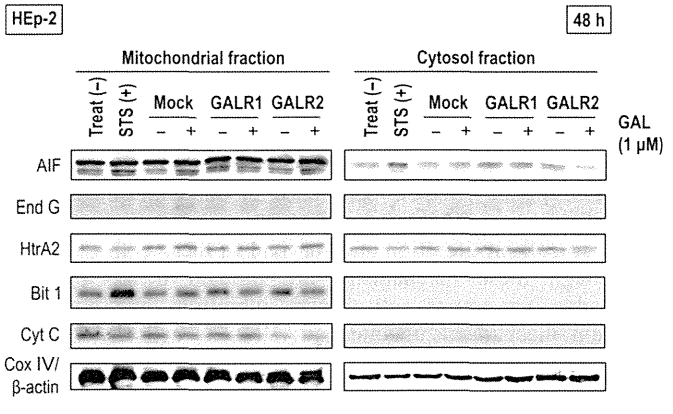

Fig. 8. Effects of mitochondrial apoptosis-associated proteins in HEp-2 cell co-administered with each of the recombinant adeno-associated virus (rAAV)-GALR vectors and galanin. Cox IV and β-actin were used as protein-loading controls for the mitochondrial and cytosolic fractions, respectively.

growth factor-dependent cell proliferation mediated by the stimulating somatostatin receptors in glioma cells.[34,35] Therefore, we anticipated that some protein phosphatase related to the dephosphorylation of MAPK cascades may be involved. As an alternative to protein phosphatase activation, Fushimi *et al.* reported that prostaglandin E2 downregulated TNF-α-induced production of matrix metalloproteinase-1 by inhibiting the Raf-1/MEK/ERK cascade through activation of the EP4 prostanoid receptor.[36] Tumor necrosis factor-α–mediated Raf activation, involving phosphorylation at Ser338, was suppressed by stimulation of the EP4 receptor; in contrast, phosphorylation of the inhibitory site on Raf, at Ser259, was stimulated via the EP4 receptor. EP4-mediated Raf inactivation was followed by dephosphorylation of MEK1/2 and ERK1/2. Hence, we examined whether GALR2 activation affects the phosphorylation state of MEK1/2, immediately upstream of ERK1/2. We confirmed that at least dephosphorylation of MEK1/2 was induced by GALR2 activation in HEp-2 cells (data not shown). A comprehensive analysis of the influence of the Ras/Raf/MEK/ERK cascades following activation of the GALR2 signaling pathway requires further study. In addition to the apoptotic mechanisms mediated by MAPK inhibition via specific inhibitors, Eisenmann *et al.* reported the importance of the MAPK pathway-downstream effector protein, RSK, and the BH-3-only proapoptotic protein Bad in melanoma cell survival.[37] Moreover, other groups reported that induction of apoptosis in melanoma cells following inhibition of MEK is mediated by the Bcl-2 family members PUMA, Bim, and Mcl-1, as well as through caspase-independent and AIF-dependent mechanism.[38,39] Therefore, we examined whether these regulators, including those belonging to the Bcl-2 and the IAP family of proteins, and caspase-dependent as well as caspase-independent apoptosis-related proteins, may be associated with the apoptotic mechanisms triggered by GALR2 activation. We found that upregulation of Bim is induced by GALR2 activation. Future studies involving downregulation of Bim expression, for instance by using siRNA, would verify this relationship further.

Although dephosphorylation of ERK1/2 by GALR2 activation was observed in both HNSCC cell lines, significant upregulation of Bim via GALR2 signaling was only induced in HEp-2, but not in KB cells. These results imply that there are both Bim-dependent and Bim-independent unknown pathways that induce apoptosis, and suggest that the type of pathways followed downstream of GALR2 depends on the cell line.

We hypothesize that the reason why the therapeutic effect of AAV-GALR2 in KB cells was less marked than in HEp-2 cells may be that KB cells do not possess the Bim-dependent pathway, whereas HEp-2 cells possess both pathways. Wittau *et al.*[40] demonstrated that there are multiple signaling pathways downstream of GALR2 in small cell lung cancer cells, resulting from coupling of GALR2 to various G-proteins. Their results supported our hypothesis that GALR2 has multiple signaling pathways by which apoptosis is induced, and that ERK inactivation, followed by upregulation of Bim, is associated with the intensity of apoptosis induction following activation of GALR2 signaling.

These findings about differences between in HEp-2 and in KB cells indicate that the pathways involved in GALR2-induced apoptosis diverge, and the details of these signaling pathways remain unclear. For further investigation, we divided GALR2-induced apoptosis pathways into caspase-dependent and -independent pathways in order to investigate this phenomenon further. When investigating the caspase-dependent pathway, we found that GALR2-inhibition of cell growth was not abrogated by the pan-caspase inhibitor z-VAD-FMK. Moreover, none of the apoptosis inducers of the caspase-independent pathway that we examined were translocated to the cytosol from the mitochondria, and activation of members of the IAP and the

Bcl-2 protein families, except for Bim, were unchanged by GALR2 signaling. These results suggested that the apoptotic pathway induced by GALR2 signaling encompasses other unknown pathways. Because carcinogenesis of HNSCC is mainly triggered by extrinsic factors, such as smoking or alcohol, which induce various genetic defects, this distinctive feature makes GALR2 advantageous as a therapeutic gene.

In conclusion, we have shown that GALR2 expression in the presence of galanin induced apoptosis via diverse pathways; thus, gene therapy using the GALR2 gene holds promise as a novel suicide-gene therapy against HNSCC.

Acknowledgments

We thank Miyoko Mitsu, Satomi Fujiwara and Mikiko Maruta for their technical assistance. This work was supported by a Grant-in-Aid for Scientific Research (Nos. 22591916, 23592539) from the Ministry of Education, Culture, Sports, Science, and Technology of Japan.

Disclosure Statement

The authors have no conflict of interest.

References

1 Kamangar F, Dores GM, Anderson WF. Patterns of cancer incidence, mortality, and prevalence across five continents: defining priorities to reduce cancer disparities in different geographic regions of the world. *J Clin Oncol* 2006; **24**: 2137–50.
2 Shibuya K, Mathers CD, Boschi-Pinto C, Lopez AD, Murray CJ. Global and regional estimates of cancer mortality and incidence by site: II. Results for the global burden of disease 2000. *BMC Cancer* 2002; **2**: 37.
3 Choong N, Vokes E. Expanding role of the medical oncologist in the management of head and neck cancer. *CA Cancer J Clin* 2008; **58**: 32–53.
4 Gold KA, Lee HY, Kim ES. Targeted therapies in squamous cell carcinoma of the head and neck. *Cancer* 2009; **115**: 922–35.
5 Tejani MA, Cohen RB, Mehra R. The contribution of cetuximab in the treatment of recurrent and/or metastatic head and neck cancer. *Biologics* 2010; **4**: 173–85.
6 Goerner M, Seiwert TY, Sudhoff H. Molecular targeted therapies in head and neck cancer–an update of recent developments. *Head Neck Oncol* 2010; **2**: 8.
7 Wang F, Arun P, Friedman J, Chen Z, Van Waes C. Current and potential inflammation targeted therapies in head and neck cancer. *Curr Opin Pharmacol* 2009; **9**: 389–95.
8 Kanazawa T, Nishino H, Hasegawa M *et al.* Interleukin-6 directly influences proliferation and invasion potential of head and neck cancer cells. *Eur Arch Otorhinolaryngol* 2007; **264**: 815–21.
9 Hill SJ. G-protein-coupled receptors: past, present and future. *Br J Pharmacol* 2006; **147**(Suppl. 1): S27–37.
10 Kanazawa T, Iwashita T, Kommareddi P *et al.* Galanin and galanin receptor type 1 suppress proliferation in squamous carcinoma cells: activation of the extracellular signal regulated kinase pathway and induction of cyclin-dependent kinase inhibitors. *Oncogene* 2007; **26**: 5762–71.
11 Kanazawa T, Kommareddi PK, Iwashita T *et al.* Galanin receptor subtype 2 suppresses cell proliferation and induces apoptosis in p53 mutant head and neck cancer cells. *Clin Cancer Res* 2009; **15**: 2222–30.
12 Lang R, Gundlach AL, Kofler B. The galanin peptide family: receptor pharmacology, pleiotropic biological actions, and implications in health and disease. *Pharmacol Ther* 2007; **115**: 177–207.
13 Mitsukawa K, Lu X, Bartfai T. Galanin, galanin receptors and drug targets. *Cell Mol Life Sci* 2008; **65**: 1796–805.
14 Berger A, Santic R, Hauser-Kronberger C *et al.* Galanin and galanin receptors in human cancers. *Neuropeptides* 2005; **39**: 353–9.
15 Iishi H, Tatsuta M, Baba M *et al.* Inhibition by galanin of experimental carcinogenesis induced by azaserine in rat pancreas. *Int J Cancer* 1998; **75**: 396–9.
16 El-Salhy M, Starefeldt A. Direct effects of octreotide, galanin and serotonin on human colon cancer cells. *Oncol Rep* 2003; **10**: 1723–8.
17 Tjomsland V, El-Salhy M. Effects of single, double or triple combinations of octreotide, galanin and serotonin on a human pancreatic cancer cell line. *Histol Histopathol* 2005; **20**: 537–41.
18 Kanazawa T, Misawa K, Carey TE. Galanin receptor subtypes 1 and 2 as therapeutic targets in head and neck squamous cell carcinoma. *Expert Opin Ther Targets* 2010; **14**: 289–302.
19 Henson BS, Neubig RR, Jang I *et al.* Galanin receptor 1 has anti-proliferative effects in oral squamous cell carcinoma. *J Biol Chem* 2005; **280**(22): 564–71.
20 Berger A, Lang R, Moritz K *et al.* Galanin receptor subtype GalR2 mediates apoptosis in SH-SY5Y neuroblastoma cells. *Endocrinology* 2004; **145**: 500–7.
21 Tofighi R, Joseph B, Xia S *et al.* Galanin decreases proliferation of PC12 cells and induces apoptosis via its subtype 2 receptor (GalR2). *Proc Natl Acad Sci USA* 2008; **105**: 2717–22.
22 Ozawa K. Gene therapy using AAV. *Uirusu* 2007; **57**: 47–55.
23 Mizukami H, Ozawa K. Utility of AAV vectors derived from novel serotypes. *Yakugaku Zasshi* 2006; **126**: 1021–8.
24 Mingozzi F, High KA. Therapeutic in vivo gene transfer for genetic disease using AAV: progress and challenges. *Nat Rev Genet* 2011; **12**: 341–55.
25 Muramatsu S, Fujimoto K, Kato S *et al.* A phase I study of aromatic L-amino acid decarboxylase gene therapy for Parkinson's disease. *Mol Ther* 2010; **18**: 1731–5.
26 Manno CS, Pierce GF, Arruda VR *et al.* Successful transduction of liver in hemophilia by AAV-Factor IX and limitations imposed by the host immune response. *Nat Med* 2006; **12**: 342–7.
27 Maguire AM, High KA, Auricchio A *et al.* Age-dependent effects of RPE65 gene therapy for Leber's congenital amaurosis: a phase 1 dose-escalation trial. *Lancet* 2009; **374**: 1597–605.
28 Kanazawa T, Mizukami H, Okada T *et al.* Suicide gene therapy using AAV-HSVtk/ganciclovir in combination with irradiation results in regression of human head and neck cancer xenografts in nude mice. *Gene Ther* 2003; **10**: 51–8.
29 Li XP, Li CY, Li X *et al.* Inhibition of human nasopharyngeal carcinoma growth and metastasis in mice by adenovirus-associated virus-mediated expression of human endostatin. *Mol Cancer Ther* 2006; **5**: 1290–8.
30 Jiang M, Liu Z, Xiang Y *et al.* Synergistic antitumor effect of AAV-mediated TRAIL expression combined with cisplatin on head and neck squamous cell carcinoma. *BMC Cancer* 2011; **11**: 54.
31 Kanter-Schlifke I, Toft Sorensen A, Ledri M, Kuteeva E, Hokfelt T, Kokaia M. Galanin gene transfer curtails generalized seizures in kindled rats without altering hippocampal synaptic plasticity. *Neuroscience* 2007; **150**: 984–92.
32 Yamada T, Horiuchi M, Dzau VJ. Angiotensin II type 2 receptor mediates programmed cell death. *Proc Natl Acad Sci USA* 1996; **93**: 156–60.
33 Huang XC, Richards EM, Sumners C. Mitogen-activated protein kinases in rat brain neuronal cultures are activated by angiotensin II type 1 receptors and inhibited by angiotensin II type 2 receptors. *J Biol Chem* 1996; **271**(15): 635–41.
34 Massa A, Barbieri F, Aiello C *et al.* The expression of the phosphotyrosine phosphatase DEP-1/PTPeta dictates the responsivity of glioma cells to somatostatin inhibition of cell proliferation. *J Biol Chem* 2004; **279**(29): 004–12.
35 Barbieri F, Pattarozzi A, Gatti M *et al.* Somatostatin receptors 1, 2, and 5 cooperate in the somatostatin inhibition of C6 glioma cell proliferation in vitro via a phosphotyrosine phosphatase-eta-dependent inhibition of extracellularly regulated kinase-1/2. *Endocrinology* 2008; **149**: 4736–46.
36 Fushimi K, Nakashima S, You F, Takigawa M, Shimizu K. Prostaglandin E2 downregulates TNF-alpha-induced production of matrix metalloproteinase-1 in HCS-2/8 chondrocytes by inhibiting Raf-1/MEK/ERK cascade through EP4 prostanoid receptor activation. *J Cell Biochem* 2007; **100**: 783–93.
37 Eisenmann KM, VanBrocklin MW, Staffend NA, Kitchen SM, Koo HM. Mitogen-activated protein kinase pathway-dependent tumor-specific survival signaling in melanoma cells through inactivation of the proapoptotic protein bad. *Cancer Res* 2003; **63**: 8330–7.
38 Panka DJ, Wang W, Atkins MB, Mier JW. The Raf inhibitor BAY 43-9006 (Sorafenib) induces caspase-independent apoptosis in melanoma cells. *Cancer Res* 2006; **66**: 1611–9.
39 Wang YF, Jiang CC, Kiejda KA, Gillespie S, Zhang XD, Hersey P. Apoptosis induction in human melanoma cells by inhibition of MEK is caspase-independent and mediated by the Bcl-2 family members PUMA, Bim, and Mcl-1. *Clin Cancer Res* 2007; **13**: 4934–42.
40 Wittau N, Grosse R, Kalkbrenner F, Gohla A, Schultz G, Gudermann T. The galanin receptor type 2 initiates multiple signaling pathways in small cell lung cancer cells by coupling to G(q), G(i) and G(12) proteins. *Oncogene* 2000; **19**: 4199–209.

Regular Article

HEMATOPOIESIS AND STEM CELLS

Overexpression of the shortest isoform of histone demethylase LSD1 primes HSPCs for malignant transformation

Taeko Wada,[1] Daisuke Koyama,[1] Jiro Kikuchi,[1] Hiroaki Honda,[2] and Yusuke Furukawa[1]

[1]Division of Stem Cell Regulation, Center for Molecular Medicine, Jichi Medical University, Tochigi, Japan; and [2]Department of Disease Model, Research Institute for Radiation Biology and Medicine, Hiroshima University, Hiroshima, Japan

Key Points

- LSD1 is barely expressed in normal hematopoietic stem cells, but is overexpressed in leukemias especially those of a T-cell origin.
- LSD1 overexpression forms preleukemic stem cells with an increased self-renewal potential in a transgenic mice model.

Recent investigations indicate that epigenetic regulators act at the initial step of myeloid leukemogenesis by forming preleukemic hematopoietic stem cells (HSCs), which possess the increased self-renewal potential but retain multidifferentiation ability, and synergize with genetic abnormalities in later stages to develop full-blown acute myeloid leukemias. However, it is still unknown whether this theory is applicable to other malignancies. In this study, we demonstrate that lysine-specific demethylase 1 (LSD1) overexpression is a founder abnormality for the development of T-cell lymphoblastic leukemia/lymphoma (T-LBL) using LSD1 transgenic mice. LSD1 expression is tightly regulated via alternative splicing and transcriptional repression in HSCs and is altered in most leukemias, especially T-LBL. Overexpression of the shortest isoform of LSD1, which is specifically repressed in quiescent HSCs and demethylates histone H3K9 more efficiently than other isoforms, increases self-renewal potential via upregulation of the HoxA family but retains multidifferentiation ability with a skewed differentiation to T-cell lineages at transcriptome levels in HSCs. Transgenic mice overexpressing LSD1 in HSCs did not show obvious abnormalities but developed T-LBL at very high frequency after γ-irradiation. LSD1 overexpression appears to be the first hit in T-cell leukemogenesis and provides an insight into novel strategies for early diagnosis and effective treatment of the disease. (*Blood*. 2015;00(00):1-15)

Introduction

Epigenetic modifications have been implicated in various biological processes of considerable importance, such as cell proliferation and differentiation.[1] Recent systematic investigations revealed that epigenetic deregulation plays fundamental roles in oncogenesis, especially the development of hematologic malignancies.[2,3] More importantly, epigenetic abnormalities generally act as initiating mutations, which transform normal stem cells into cancer stem cells at the initial step of oncogenesis. For example, recurrent mutations of DNA methyltransferase 3A (DNMT3A) or isocitrate dehydrogenase (IDH) 1/2 give rise to preleukemic hematopoietic stem cells (HSCs), which possess a higher self-renewal potential than normal counterparts but retain multidifferentiation capacity.[4-6] Additional genetic abnormalities, such as NPM1c mutations and FLT3-internal tandem duplication, confer further growth advantages and malignant phenotypes to preleukemic HSCs, leading to the development of full-blown acute myeloid leukemias (AML). Similar initiator functions have been demonstrated in other epigenetic regulators, such as the methylcytosine hydroxylase TET2, histone methyltransferase EZH2, and Polycomb-related protein ASXL2, in myeloid leukemogenesis.[7-10] However, it is still unknown whether this theory is applicable to other malignancies.

Lysine-specific demethylase 1 (LSD1 also named KDM1A/AOF2/BHC110) is an FAD-dependent histone demethylase that specifically removes the monomethyl and dimethyl groups from lysine-4 and lysine-9 residues of histone H3.[11] Hence, LSD1 bifunctionally modulates the enhancer/promoter functions of target genes in a context-dependent manner.[12] LSD1 mediates a repressive function via H3K4 demethylation as a component of the CoREST and NuRD complexes,[13] whereas it activates hormone-regulated genes via H3K9 demethylation when associated with androgen or estrogen receptors.[14] Moreover, LSD1 has 4 isoforms with different histone demethylating activities and affinities to CoREST, offering an additional layer of functional regulation.[15]

Recent genetic approaches revealed that LSD1 is indispensable for broad tissue homeostasis and proper development.[16] In the hematopoietic system, Sprüssel et al[17] demonstrated that shRNA-mediated knockdown of LSD1 impairs maturation of blood cells in association with the expansion of undifferentiated hematopoietic stem/progenitor cells (HSPCs) and committed progenitors in mice.

Submitted November 6, 2014; accepted April 15, 2015. Prepublished online as *Blood* First Edition paper, April 22, 2015; DOI 10.1182/blood-2014-11-610907.

The microarray data reported in this article have been deposited in the MIAME-compliant Gene Expression Omnibus database (accession number GSE66074).

The online version of this article contains a data supplement.

The publication costs of this article were defrayed in part by page charge payment. Therefore, and solely to indicate this fact, this article is hereby marked "advertisement" in accordance with 18 USC section 1734.

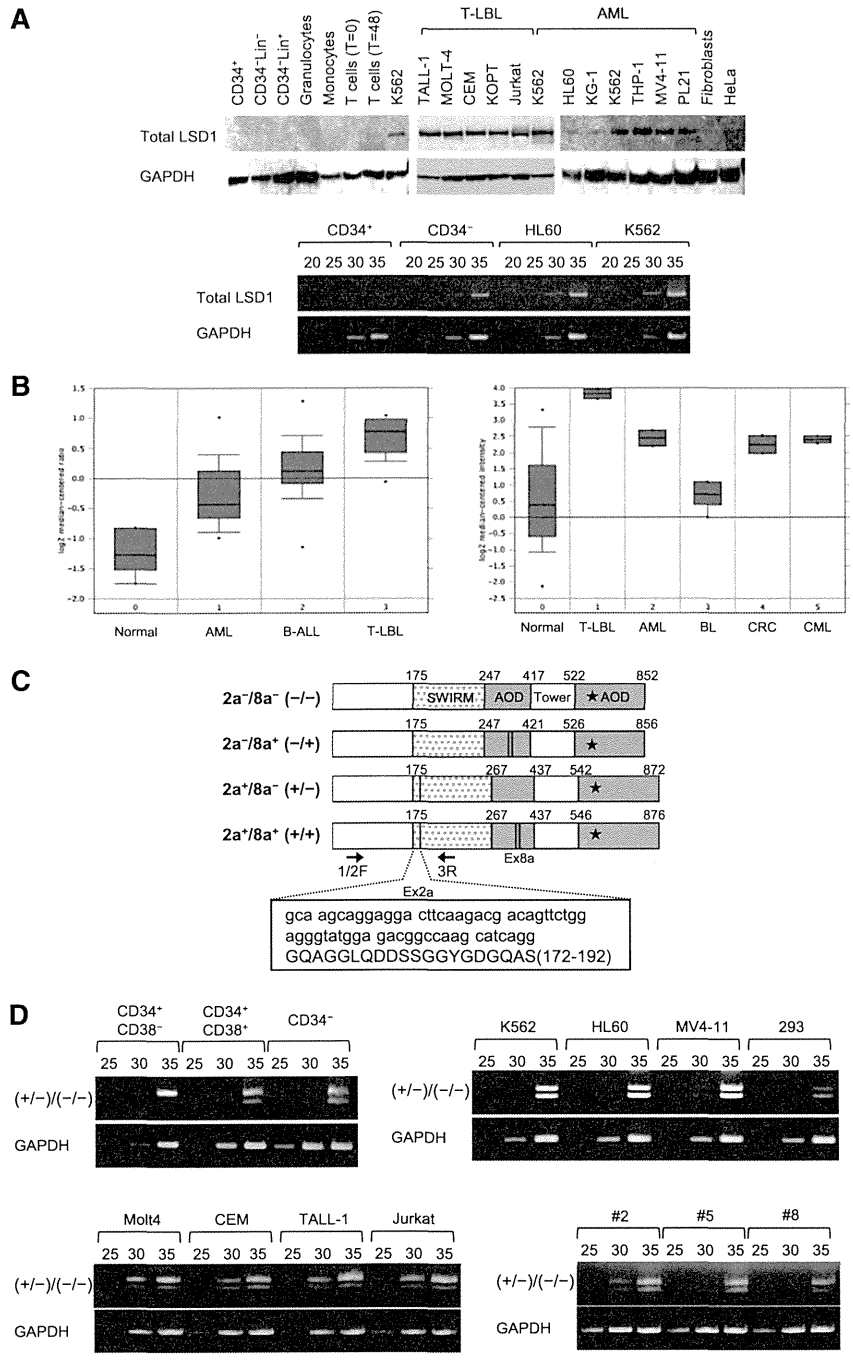

Figure 1. LSD1 is barely expressed in normal HSPCs, but is overexpressed in leukemic cells. (A) Top panel, We isolated whole-cell lysates from normal human bone marrow cells ($CD34^+$ HSPCs, $CD34^-/Lin^-$ progenitors, and Lin^+ cells), mature blood cells (granulocytes, monocytes, uncultured T lymphocytes, and 24-hour–stimulated T lymphocytes), T-LBL cell lines (TALL-1, MOLT-4, CEM, KOPT-K1, and Jurkat), myeloid leukemia cell lines (K562, HL-60, KG-1, THP-1, MV4-11, and PL-21), normal human fibroblasts, and the cervical carcinoma cell line HeLa for immunoblot analyses on the expression of LSD1 and GAPDH (internal control). Bottom panel, We isolated total cellular RNA from the indicated cells and subjected them to semiquantitative RT-PCR analysis for the expression of LSD1 and GAPDH. The PCR products of suboptimal amplification cycles, 20 to 35 cycles, were electrophoresed (5 μL per lane). (B) LSD1 mRNA expression in primary samples according to the Oncomine database (http://www.oncomine.org). Left panel: 0, normal bone marrow mononuclear cells (n = 6); 1, AML (n = 23); 2, B-cell acute lymphoblastic leukemia (n = 87); 3, T-LBL (n = 11). Right panel: 0, various normal somatic cells (n = 146); 1, T-LBL (n = 2); 2, AML (n = 2); 3, Burkitt lymphoma (n = 4); 4, colorectal cancer (n = 2); 5, chronic myelogenous leukemia (n = 2). $^*P < .05$ determined by a 1-way ANOVA with the Bonferroni post hoc test. (C) The structure of 4 LSD1 isoforms generated by either the single or double inclusion of 2 alternative exons 2a (Ex2a) and 8a (Ex8a). *The FAD-binding domain. We designed PCR primers 1/2F and 3R (arrows) to detect LSD1 isoforms ($^{-/-}$) and ($^{+/-}$) discriminately based on differences in sizes (60 bp as shown in the box). (D) We performed semiquantitative RT-PCR for the expression of LSD1 isoforms in normal human hematopoietic progenitors, leukemic cell lines, and primary T-LBL cells from 3 patients (cases 2, 5, and 8). The cDNAs were amplified with primers covering the entire exons (1F and 19R; see supplemental Table 1 for nucleotide sequences), followed by nested PCR with primers 1/2F and 3R as reported by Zibetti et al.[15] (E) The signal intensities of each band at 35 cycles in panel D were quantified by NIH Image J software, normalized to those of corresponding GAPDH, and shown as relative values setting the expression level of LSD1 ($^{-/-}$) in $CD34^+/CD38^-$ cells to 1.0. (F) We quantified the mRNA expression of total LSD1, mostly ($^{-/-}$) and ($^{+/-}$), with 1/2F and 3R primers and the isoform ($^{+/-}$) with 1/2F and 2aR (within exon 2a) primers using the Power SYBR Green PCR Master Mix (Life Technologies). The expression level was normalized to that of GAPDH and quantified by the $2^{-\Delta\Delta Ct}$ method. The means ± SD (bars) of 3 independent experiments are shown. (G) We isolated total cellular RNA from murine $Lin^-/Sca\text{-}1^+/c\text{-}Kit^+$ and $Lin^-/Sca\text{-}1^-/c\text{-}Kit^+$ cells, and subjected them to nested RT-PCR for the expression of murine LSD1 isoforms with primer pairs of 2F and 3R (top panel) or 2F and 8/9R (middle panel) (see supplemental Table 1 for nucleotide sequences). ANOVA, analysis of variance; CT, cycle threshold; SD, standard deviation.

Q:16

On the other hand, LSD1 was shown to be essential for the self-renewal and proper differentiation of HSCs in conditional LSD1 knockout mice.[18] Furthermore, it is of note that LSD1 expression is elevated in neuroblastoma and bladder cancer[19,20] and is correlated with a poor prognosis in hormone-dependent prostate and breast cancers.[21]

From these observations, we hypothesized that the expression levels and function of LSD1 are tightly regulated in HSPCs and their deregulation underlies the development of hematologic malignancies. This idea is compatible with the initiating role of epigenetic deregulation in leukemogenesis, but has not yet been experimentally proven. In the present study, we investigated whether the abnormalities of LSD1 cause the malignant transformation of HSPCs by generating transgenic mice that overexpress an LSD1 isoform in HSPCs under the control of the Sca-1 promoter.

Methods

Cells

Human bone marrow mononuclear cells and $CD34^+$ progenitors were purchased from Takara Bio. $CD34^-$/lineage markers $(Lin)^-$ and $CD34^-/Lin^+$ cells were separated with CD34 microbeads and lineage cell depletion kits (Miltenyi

Figure 1. (Continued).

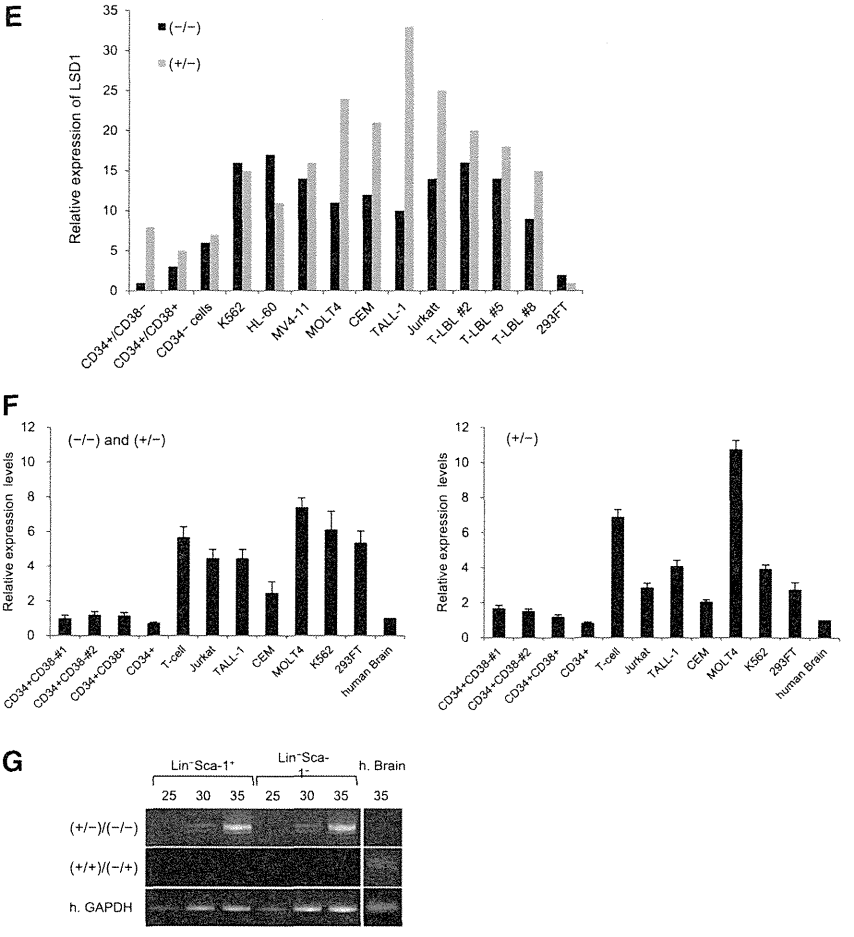

Biotec). $CD34^+/CD38^+$ and $CD34^+/CD38^-$ cells were purified with an anti-human CD38 antibody in the Easy Sep system (StemCell Technologies). Leukemic cell lines were handled as described previously.[22] Primary leukemic cells were isolated at the time of diagnostic procedure from patients after obtaining informed consent in accordance with the Declaration of Helsinki and the protocol approved by the institutional review board of Jichi Medical University. We used specimens containing >90% blasts on morphological and phenotypic examinations. Fractionation of murine HSCs and HSPCs was performed according to the protocol of Oguro et al.[23]

Colony formation and replating assays

Purified $Lin^-/Sca\text{-}1^+/c\text{-}Kit^+$ (LSK) and $Lin^-/Sca\text{-}1^-/c\text{-}Kit^+$ cells (5×10^5 cells) were plated in triplicate in methylcellulose M3231 medium (StemCell Technologies) supplemented with stem cell-oriented cytokines. The colony number was scored after 7 days, followed by second and third platings.

Polymerase chain reaction

Q:10 We performed reverse transcription–polymerase chain reaction (RT-PCR) and real-time quantitative RT-PCR as described previously.[15,24] TCRβ rearrangement was analyzed by genomic PCR according to Shen et al.[25] Primer sequences are listed in supplemental Table 1 (see supplemental Data available at the *Blood* Web site).

Plasmids and transfection

Full-length complementary DNAs (cDNAs) for LSD1 transcript variants 1 (BC040194, $E2a^+/E8a^+$) and 2 (BC048134, $E2a^-/E8a^-$) were purchased from Open Biosystems. We constructed cDNA for LSD1 isoform $E2a^+/E8a^-$ from variants 1 and 2 as described by Zibetti et al.[15] Lentiviral expression vectors were constructed by inserting full-length cDNAs into a CSII-CMV-MCS-IRES DsRed vector as reported.[26]

Immunoblotting

We carried out immunoblotting using specific antibodies against LSD1 (Diagenode and Cell Signaling Technology), G9a, Suv39H1 (Cell Signaling Technology), PHF8/JHDM1F (Active Motif), JARID1B (Sigma-Aldrich), dimethylated H3K4 (Active Motif), dimethylated H3K9 (Abcam), histone H3, and glyceraldehyde-3-phosphate dehydrogenase (GAPDH; Cell Signaling Technology).

In vitro histone demethylase assay

In vitro translated LSD1[27] (0-20 μg) was incubated with 8 μg of calf thymus histones (Roche) or 0.3 μg of purified HeLa mononucleosomes (EpiCypher) with or without 3.9 μM recombinant CoREST (BPS BioScience), followed by immunoblotting using methyl-specific antibodies.

Mice

To generate the LSD1 transgenic mice C57BL/6J-Tg(Ly6a-KDM1A*v2), human LSD1 cDNA encoding the shortest isoform ($E2a^-/E8a^-$) and an SV40 early polyadenylation (pA) signal were inserted into the Ly-6A cassette (pLy-6A14) that contains the mouse Sca-1 gene and its regulatory regions.[28] The DNA fragment containing the mouse Sca-1 promoter and human LSD1 cDNA with a pA signal was excised with *Not*I and microinjected into the pronuclei of C57BL/6 mice as described.[29] The copy number of the transgene was determined by blotting mouse tail DNA with human LSD1 cDNA as a probe and comparing

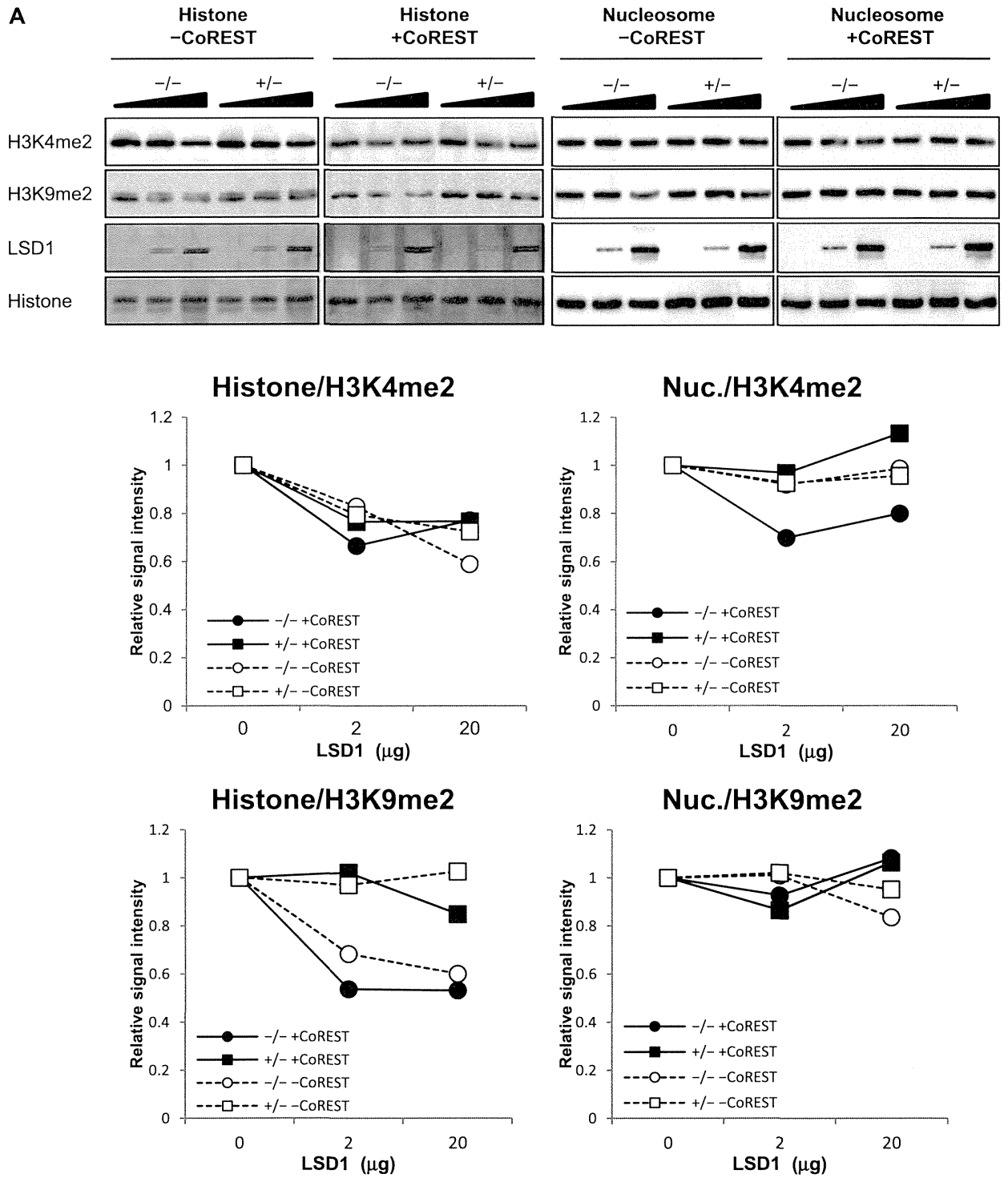

Figure 2. Differential functions of LSD1 isoforms. (A) Calf thymus histones or HeLa mononucleosomes were incubated with purified LSD1 (0, 2, and 20 μg) with or without recombinant CoREST, followed by immunoblotting using specific antibodies or silver staining (LSD1 and histones) (top panel). Signal intensities were quantified and shown as relative values of corresponding untreated controls (bottom panel). (B) Whole-cell lysates were prepared from HEK293 cells transfected with expression vectors for LSD1 isoform ($^{-/-}$) or ($^{+/-}$), and subjected to immunoblotting with the indicated antibodies. Signal intensities were quantified and shown as relative values of corresponding mock transfectants. (C) LSD1 expression and activity in HSPCs (see text for detail).

Q:17

the band intensity with copy controls of the injection fragment. Pathological examination of mice was conducted by outside experts. All animal studies were approved by the Institutional Animal Ethics Committee and performed in accordance with the Guide for the Care and Use of Laboratory Animals formulated by the National Academy of Sciences.

Stem cell transplantation in syngeneic mice

Bone marrow mononuclear cells were isolated from LSD1 transgenic and control mice at 8 to 12 weeks of age, and injected via the tail vein into lethally irradiated (9.5 Gy) C57BL/6 (CD45.1) recipient mice (8-12 weeks of age)

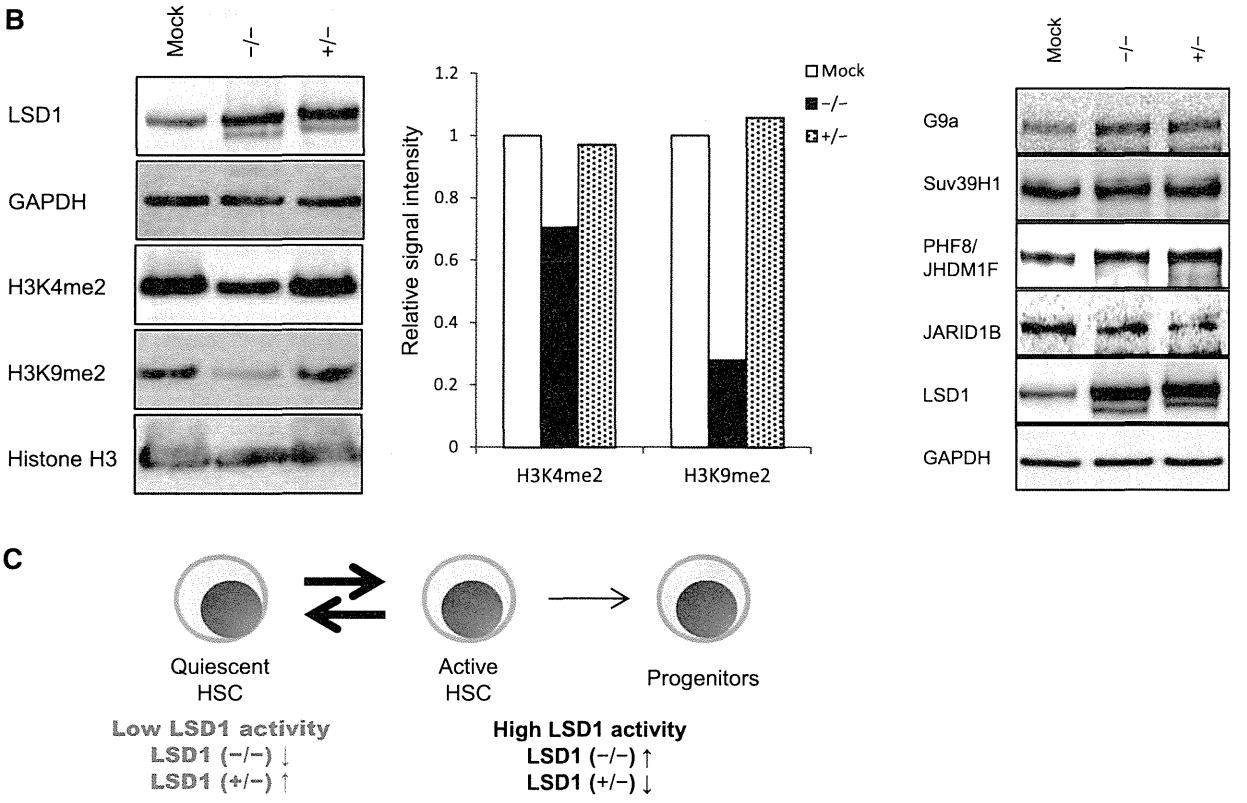

Figure 2. (Continued).

with 2×10^5 backup cells.[30] Engraftment was confirmed by measuring the percentage of $CD45.2^+$ cells in the peripheral blood. Subsequent transplantations were similarly performed using 2×10^6 bone marrow cells with a 12-week interval.

Cell cycle analysis in vivo

Bone marrow cells were harvested 40 minutes after IP injection of bromodeoxyuridine (1.5 mg/150 μL) and stained with the APC BrdU Flow kit (BD Pharmingen) to determine cell cycle distribution on flow cytometry.

Global analysis of messenger RNA expression

RNA samples (3 μg) were labeled using T4 RNA ligase in duplicate, and hybridized with the Gene Chip Mouse Genome 430 2.0 Array (Affymetrix). The hybridized arrays were scanned with a GeneChip Scanner 3000, and the scanned images were processed using GeneChip operating software (Affymetrix).

Results

LSD1 is barely expressed in normal HSPCs, but is overexpressed in leukemic cells

In an initial effort to clarify the role of LSD1 in leukemogenesis, we compared the expression of LSD1 between normal human hematopoietic cells and leukemic cell lines at protein and messenger RNA (mRNA) levels. LSD1 protein was under the detection limit in normal human hematopoietic cells including $CD34^+$ HSPCs, $CD34^-$ bone marrow progenitors, lineage marker-positive bone marrow cells, and mature blood cells (Figure 1A top panel). LSD1 expression was also very low in $CD34^+$ HSPCs but was slightly upregulated in $CD34^-/Lin^-$ progenitors at the mRNA level (Figure 1A bottom panel). In contrast, LSD1 was strongly expressed in most leukemic cell lines, especially those derived from T-lymphoblastic leukemia/lymphoma (T-LBL) and those harboring leukemic fusion proteins such as K562 (BCR-ABL^+), THP-1 (MLL-$AF9^+$), MV4-11 (MLL-$AF4^+$), and PL-21 (PMA-$RAR\alpha^+$) (Figure 1A top panel). LSD1 overexpression was confirmed at the mRNA level in leukemic cell lines (Figure 1A bottom panel). In addition, we analyzed LSD1 mRNA expression in primary samples using published data sets from the Oncomine microarray database and verified LSD1 overexpression in primary leukemic cells relative to normal bone marrow cells. Consistent with the results of the cell line studies, LSD1 expression was the highest in primary T-LBL cells, followed by BCR-ABL carrying chronic myelogenous leukemia and AML in primary samples (Figure 1B).

LSD1 isoforms are differentially expressed in normal HSCs and leukemic cells

Mammals have 4 LSD1 isoforms generated by either the single or double inclusion of 2 alternative exons 2a and 8a, which are located in the SWIRM and amine oxidase domains, respectively (Figure 1C). Although the neuron-specific expression of exon 8a-retaining splice variants has been reported previously,[15] no information is available regarding the expression pattern and biological functions of LSD1 isoforms in the hematopoietic system. To address this issue, we attempted to detect LSD1 isoforms discriminately using isoform-specific RT-PCR (supplemental Table 1). Hematopoietic cells expressed the isoform ($^{-/-}$), which

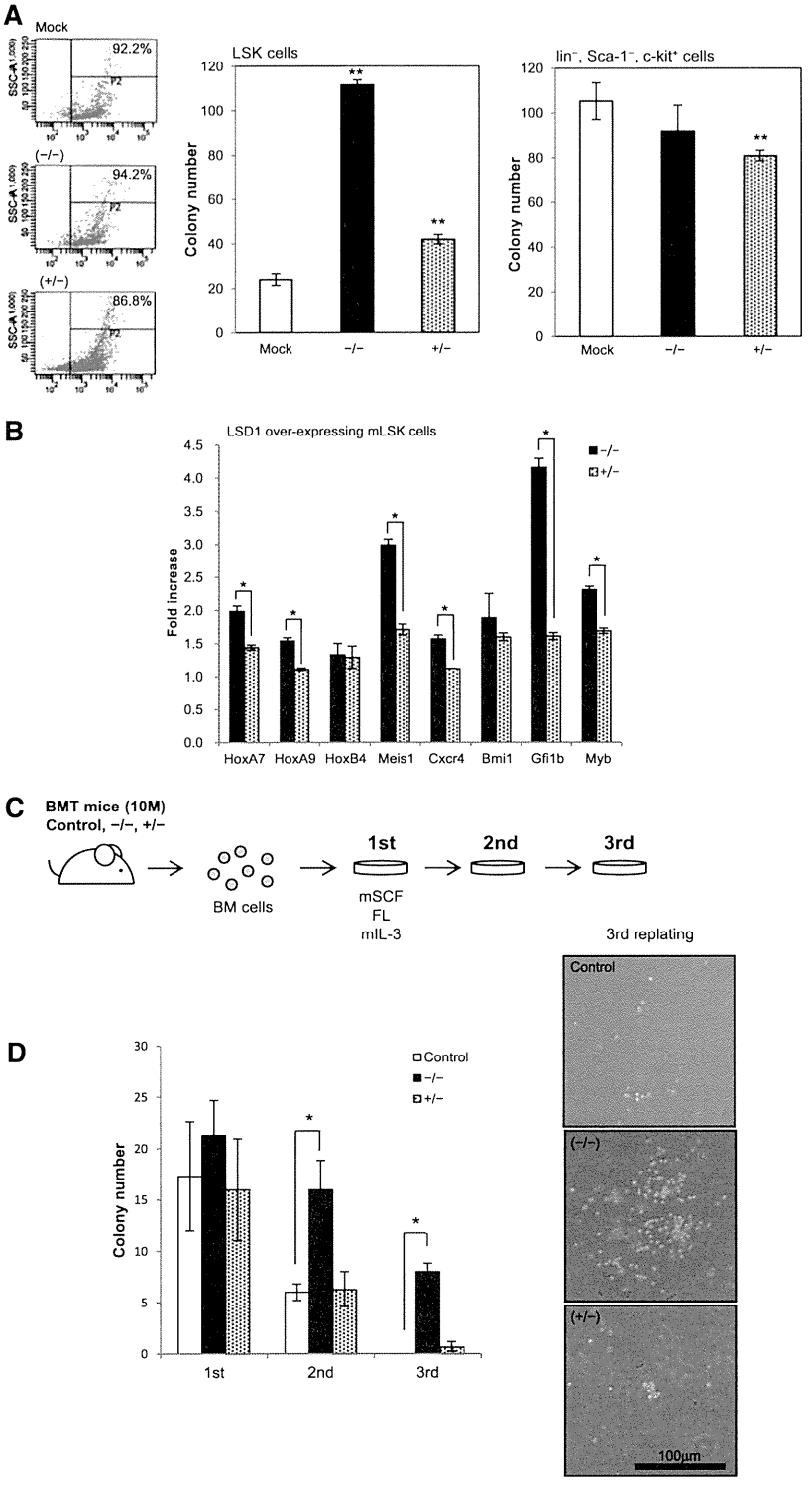

Figure 3. The shortest isoform of LSD1 positively regulates the self-renewal of HSCs. (A) We transduced LSK and Lin$^-$/Sca-1$^-$/c-Kit$^+$ cells from normal mouse bone marrow with an empty plasmid (Mock) or expression vectors for LSD1 isoforms ($^{-/-}$) and ($^{+/-}$) for 48 hours, and cultured them in methylcellulose medium for 7 days to evaluate the clonogenic growth. Signal intensity of DsRed is shown in the left panel as a surrogate marker of LSD1 expression in starting materials. (B) Total cellular RNA was isolated from LSK cells transduced with LSD1 isoforms ($^{-/-}$) or ($^{+/-}$), and subjected to real-time quantitative RT-PCR for the expression of the indicated genes. Data were quantified by the $2^{-\Delta\Delta Ct}$ method using simultaneously amplified GAPDH as a reference and shown as fold increases against mock-transfected controls. (C) c-Kit–positive bone marrow mononuclear (BM) cells were transduced with an empty vector (Control), LSD1 isoform ($^{-/-}$) or ($^{+/-}$), and transplanted into lethally irradiated recipient mice. We isolated bone marrow mononuclear cells from recipient mice 10 months after transplantation and performed colony-replating assays in the presence of murine stem cell factor (mSCF), FLT3 ligand (FL), and murine interleukin-3 (IL-3) at 50, 50, and 10 ng/mL, respectively. (D) The means ± SD (bars) of colony numbers in each passage (left panel) and representative photographs of colonies (right panel) are shown. $^*P < .01$ and $^{**}P < .05$ determined by a 1-way ANOVA with the Bonferroni post hoc test (n = 3).

carries no additional exons, and the isoform ($^{+/-}$), which has the insertion of exon 2a (Figure 1D). Neuron-specific isoforms ($^{+/+}$) and ($^{-/+}$) were undetectable in either normal or malignant hematopoietic cells (supplemental Figure 1A). Among normal bone marrow cells, the isoform ($^{-/-}$) was barely detected in CD34$^+$/CD38$^-$ HSCs and was upregulated in CD34$^+$/CD38$^+$ multipotent progenitors and CD34$^-$/Lin$^-$ committed progenitors by semi-quantitative RT-PCR (Figure 1D-E) and real-time quantitative RT-PCR (Figure 1F). In contrast, leukemic cells, including primary samples from 3 patients with T-LBL, apparently overexpressed both ($^{-/-}$) and ($^{+/-}$) forms (Figure 1D-F). Finally, we investigated whether the same expression pattern of LSD1 isoforms is retained in murine HSPCs. The isoform ($^{-/-}$) was faintly expressed in LSK and Lin$^-$/Sca-1$^-$/c-Kit$^+$ fractions, as observed in human CD34$^+$/CD38$^-$ HSCs, whereas the expression of the isoform ($^{+/-}$) was relatively strong (Figure 1G). Neuron-specific

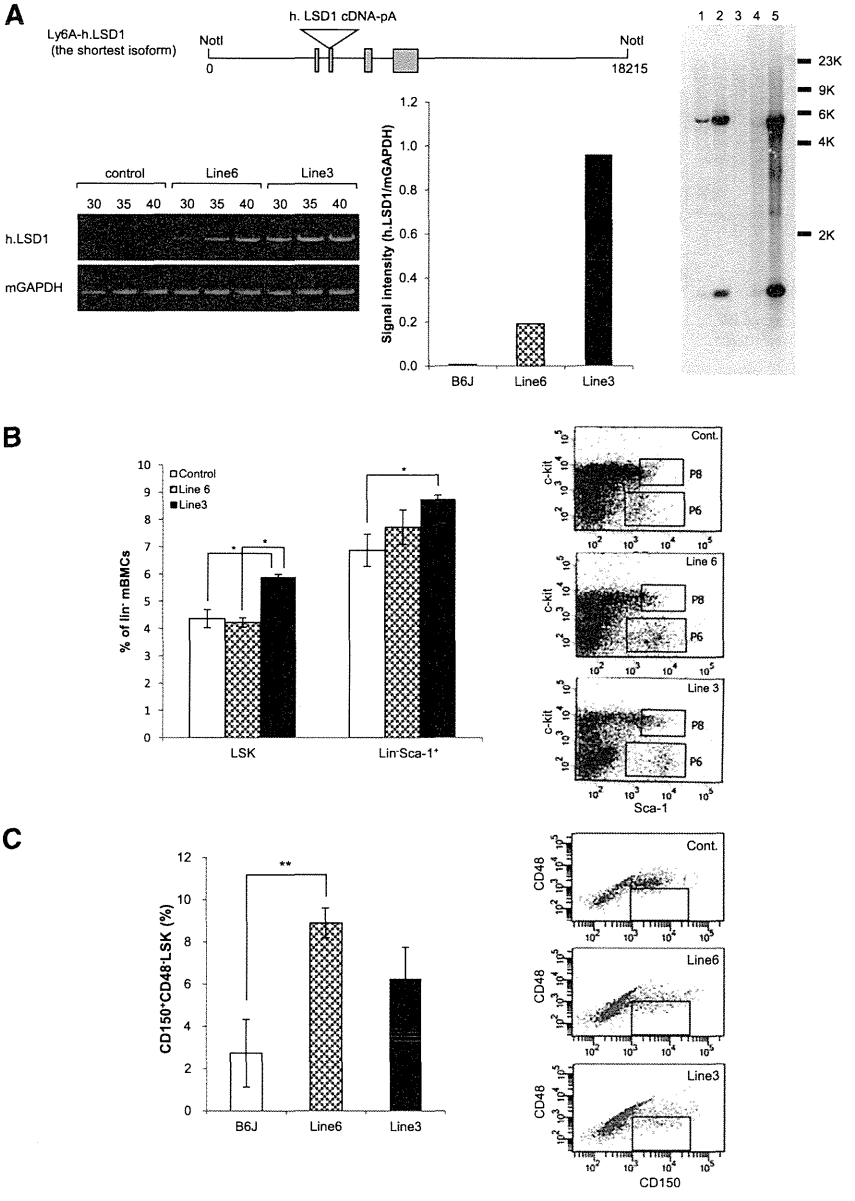

Figure 4. The shortest isoform of LSD1 enhances the stemness and self-renewal of HSPCs in vivo. (A) Top panel, Schematic view of the injected fragment for the generation of LSD1 transgenic mice. Bottom panel, We quantified the expression of human LSD1 and murine GAPDH (internal control) transcripts in 2 lines of LSD1 transgenic and B6J (Control) mice using specific primers (supplemental Table 1). Right panel, Genomic DNA (5 μg) was digested with *Bam*HI and hybridized with LSD1 cDNA as a probe to estimate copy numbers of transgene. Lane 1, DNA from wild-type mice + 2 copies of the injection fragment; lane 2, DNA from wild-type mice + 20 copies of the injection fragment; lane 3, DNA from wild-type mice; lane 4, DNA from line 6 mice; lane 5, DNA from line 3 mice. (B) We determined the percentage of LSK and $Lin^-/Sca\text{-}1^+$ cells in the bone marrow of 2 lines of LSD1 transgenic and B6J (Control) mice using flow cytometry. Representative data are shown in the right panel (P8 and P6 correspond to LSK and $Lin^-/Sca\text{-}1^+$ fractions, respectively). (C) We determined the percentage of $CD150^+/CD48^-$ cells in LSK fractions of 2 lines of LSD1 transgenic and B6J mice using flow cytometry. Representative data are shown in the right panel (the boxed area corresponds to $CD150^+/CD48^-/LSK$ fractions). (D) We determined the cell cycle profile of $Lin^-/Sca\text{-}1^+$ and Lin^- bone marrow mononuclear cells in 2 lines of LSD1 transgenic and B6J (Control) mice in vivo. (E) Bone marrow cells from 2 lines of LSD1 transgenic and B6J (Control) mice (CD45.2) were transplanted into lethally irradiated C57BL/6 (CD45.1) mice. We determined the percentage of $CD45.2^+$ cells in the peripheral blood 24 weeks after transplantation. (F) Bone marrow cells were collected from control- and LSD1-recipient mice 12 weeks after primary transplantation, and transplanted into lethally irradiated C57BL/6 mice. Tertiary transplantation was similarly performed 12 weeks after secondary transplantation. The means ± SD (bars) of 3 independent experiments are shown. $^*P < .05$ and $^{**}P < .01$ determined by 1-way ANOVA with the Bonferroni post hoc test. (G) Cell cycle status of HSPCs in LSD1 transgenic mice (see text for detail).

isoforms ($^{+/+}$) and ($^{-/+}$) were also undetectable in murine hematopoietic cells.

The shortest isoform of LSD1 displays robust histone H3K9 demethylating activity in vivo

To gain insights into functional differences between the LSD1 isoforms, we compared histone demethylating activity of the 2 isoforms in vitro and in vivo. The in vitro histone demethylation assay revealed that the isoform ($^{-/-}$) readily demethylated both H3K4 and H3K9 in naked histones even in the absence of CoREST, whereas the isoform ($^{+/-}$) had little if any H3K9 demethylating activity and weak H3K4 demethylating activity (Figure 2A left half). The same assay using nucleosomes yielded slightly different results: H3K4 demethylation was detected only with the isoform ($^{-/-}$) in the presence of CoREST and very weak H3K9 demethylation was observed with the isoform ($^{+/-}$) in the absence of CoREST (Figure 2A right half). As the experiments with nucleosomes might reflect the in vivo situation more accurately, we attempted to confirm these results by analyzing the methylation status of endogenous histones in HEK293 cells after the overexpression of each isoform. The isoform ($^{-/-}$) demethylated H3K9 robustly and H3K4 moderately, whereas the isoform ($^{+/-}$) displayed very weak activity for both residues in HEK293 cells (Figure 2B left panel; supplemental Figure 1B). The discrepancy between the results of in vitro demethylation and in vivo transfection assays might be due to the effects of LSD1 on other histone modification enzymes. To investigate this possibility, we examined the expression of H3K9 methyltransferases G9a and Suv39H1, H3K9 demethylase PHF8/JHDM1F and H3K4 demethylase JARID1B in LSD1-overexpressing HEK293 cells. As shown in Figure 2B (right panel), LSD1 readily increased and decreased the expression levels of PHF8/JHDM1F and JARID1B, respectively. Combined with the expression data, we propose the model that low LSD1 activity is required to maintain HSCs in a quiescent state and an increase in LSD1 activity, especially that against H3K9, via the upregulation of the isoform ($^{-/-}$) shifts quiescent HSCs to an active/cycling state (Figure 2C).